Electronic Supplementary Information

Bipolar redox electrolytes-synergistically mediated NiCoMn-811 high-Ni ternary perovskite fluorides for advanced supercapacitors in both alkaline and neutral media†

Wei Shi,[1a] Wujiang Yu,[1a] Rui Ding,*[a] Ziyang Jia,[a] Yi Li,[a] Yuxi Huang,[a] Caini Tan,[a] Xiujuan Sun,[a] and Enhui Liu[a]

[a] *Key Laboratory of Environmentally Friendly Chemistry and Applications of Ministry of Education, College of Chemistry, Xiangtan University (XTU), Xiangtan, Hunan, 411105, P.R. China. Emails: drm8122@163.com ; drm8122@xtu.edu.cn*

[1] *The authors contribute equally to the work.*

Table of Contents

$[Cu(NH_3)_4]^{2+}$ additive.

Fig. S15 The CV plots at 2-160 mV s^{-1} (Inset shows the plots of lg*v*-lg*i*) (a) and GCD curves at 1-32 A g^{-1} (b) of the 8# electrode in 3 M KNO_3 (C)+10 mM $K_3[Fe(CN)_6]$; the CV plots at 10-160 mV s^{-1} (Inset shows the plots of lg*v*-lg*i*) (c) and GCD curves at 1-64 A g^{-1} (d) of AC electrode in 3 M KCl (B)+10 mM $[Cu(NH_3)_4]^{2+}$.

Fig. S16 Pseudocapacitive/diffusion contribution ratio (a) and the CV area for pseudocapacitive part in the CV plots at 2-20 mV s^{-1} of the 8# electrode in 3 M KNO_3 (C) electrolytes with 10 mM $[Fe(CN)_6]^{3-}$ additives.

Fig. S17 The CV area for pseudocapacitive part in the CV plots (a-e) and pseudocapacitive/diffusion contribution ratio (f) at 10-160 mV s^{-1} of the AC electrode in 3 M KCl (B) electrolytes with10 mM $[Cu(NH_3)_4]^{2+}$ additives.

Fig. S18 The detail drawing for H-type SC structure

Fig. S19 The CV window (a, d, g), CV plots of 10-160 mV s^{-1} (b, e, h) and GCD curves at 1–32 A g^{-1} (c, f, i) of Ⅰ, Ⅱ and Ⅲ H-type capacitors

Ⅰ: AC (A+10 mM $[Cu(NH_3)_4]^{2+}$) //811-8# (A+10 mM $[Fe(CN)_6]^{3-}$)

Ⅱ: AC (A+10 mM $[Cu(NH_3)_4]^{2+}$) // 811-8# (A+20 mM $[Fe(CN)_6]^{3-}$)

Ⅲ: AC (B+10 mM $[Cu(NH_3)_4]^{2+}$) // 811-8# (A+10 mM $[Fe(CN)_6]^{3-}$)

Fig. S20 The CV window (a, d, g), CV plots of 10-160 mV s^{-1} (b, e, h) and GCD curves at 1–32 A g^{-1} (c, f, i) of Ⅳ, Ⅴ and Ⅵ H-type capacitors

Ⅳ: AC (A+10 mM $[Cu(NH_3)_4]^{2+}$) // 811-8# (C+10 mM $[Fe(CN)_6]^{3-}$)

Ⅴ: AC (B+10 mM $[Cu(NH_3)_4]^{2+}$) // 811-8# (C+10 mM $[Fe(CN)_6]^{3-}$)

Ⅵ: AC (A) // 811-8# (A)

Fig. S21 The CV window (a, d), CV plots of 10-160 mV s^{-1} (b, e) and GCD curves at 1–32 A g^{-1} (c, f) of Ⅰ H-type capacitor with high and low temperatures.

Fig. S22 The CV window (a, d, g, j, m), CV plots of 10-160 mV s^{-1} (b, e, h, k, n) and GCD curves at 1–32 A g^{-1} (c, f, i, l, o) of Ⅶ-Ⅺ H-type capacitors under high temperature.

Ⅶ: AC (A+10 mM $[Cu(NH_3)_4]^{2+}$) // 811-8# (A+10 mM $[Fe(CN)_6]^{3-}$+0.5% Na_2MoO_4)

Ⅷ: AC (A+10 mM $[Cu(NH_3)_4]^{2+}$) // 811-8# (A+10 mM $[Fe(CN)_6]^{3-}$+1.0% Na_2MoO_4)

Ⅸ: AC (A+10 mM $[Cu(NH_3)_4]^{2+}$) //811-8# (A+10 mM $[Fe(CN)_6]^{3-}$+1.5% Na_2MoO_4)

Ⅹ: AC (A+10 mM $[Cu(NH_3)_4]^{2+}$) // 811-8# (A′+10 mM $[Fe(CN)_6]^{3-}$+1.0% Na_2MoO_4)

ⅩⅠ: AC (A+10 mM $[Cu(NH_3)_4]^{2+}$) // 811-8# (A″+10 mM $[Fe(CN)_6]^{3-}$+1.0% Na_2MoO_4).

Fig. S23 The EDS data of the 8# cathode in the Ⅷ H-type capacitor [AC (A+10 mM $[Cu(NH_3)_4]^{2+}$) // 811-8# (A+10 mM $[Fe(CN)_6]^{3-}$+1.0% Na_2MoO_4)] after the cycling tests under high temperature.

Table S1 The orthogonal analysis of KNCMF-811(1#-9#) electrodes in A electrolytes

Table S2 Specific capacity (C g^{-1}) and cycling retention (%) of the KNCMF-811 (1#-9#) and AC electrodes in A electrolytes.

Table S3. EIS fitting parameters of the 8# electrode before and after cycling test in A electrolytes.

Table S4 The preparation of specific electrolytes.

Table S5. Specific capacity (C g^{-1}) and cycling retention (%) of the 8# electrode in A electrolytes with different concentrations of $[Fe(CN)_6]^{3-}$ additives.

Table S6 Specific capacity (C g^{-1}) and cycling retention (%) of the AC electrode in A electrolytes with different concentrations of $[Cu(NH_3)_4]^{2+}$ additives.

Table S7 The active mass ratios of AC anode/811-8# cathode for SCs

Table S8 The specific electrolytes of AC anode and 811-8# cathode for SCs

Table S9 Ragone and cycling behavior of SCs at room temperature.

Table S10. A comparison for the performance of the SCs in the study with some reported SCs.

Table S11 Ragone and cycling behavior of SCs at low and high temperatures.

Table S12 Chemicals, reagents and materials used in the study.

References

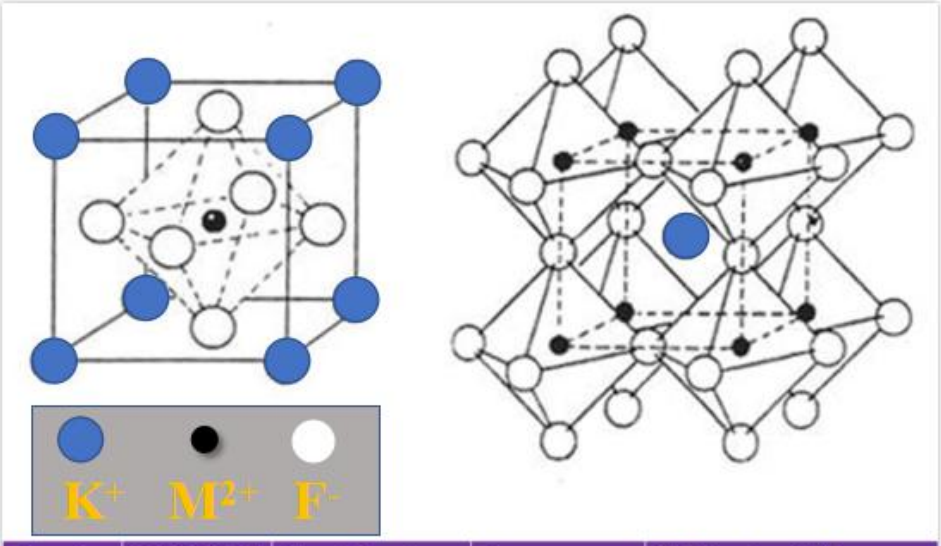

Sample	ICCD-PDF	Crystal system	Space group	Cell (a×b×c)/Å^3
$KNiF_3$	21-1002	Cubic	Pm-3m	4.0127×4.0127×4.0127
$KCoF_3$	18-1006	Cubic	Pm-3m	4.0708×4.0708×4.0708
$KMnF_3$	17-0116	Cubic	Pm-3m	4.189×4.189×4.189

Fig. S1 The crystalline structures of perovskite KMF_3 and crystalline parameters for $KNiF_3$, $KCoF_3$ and $KMnF_3$.

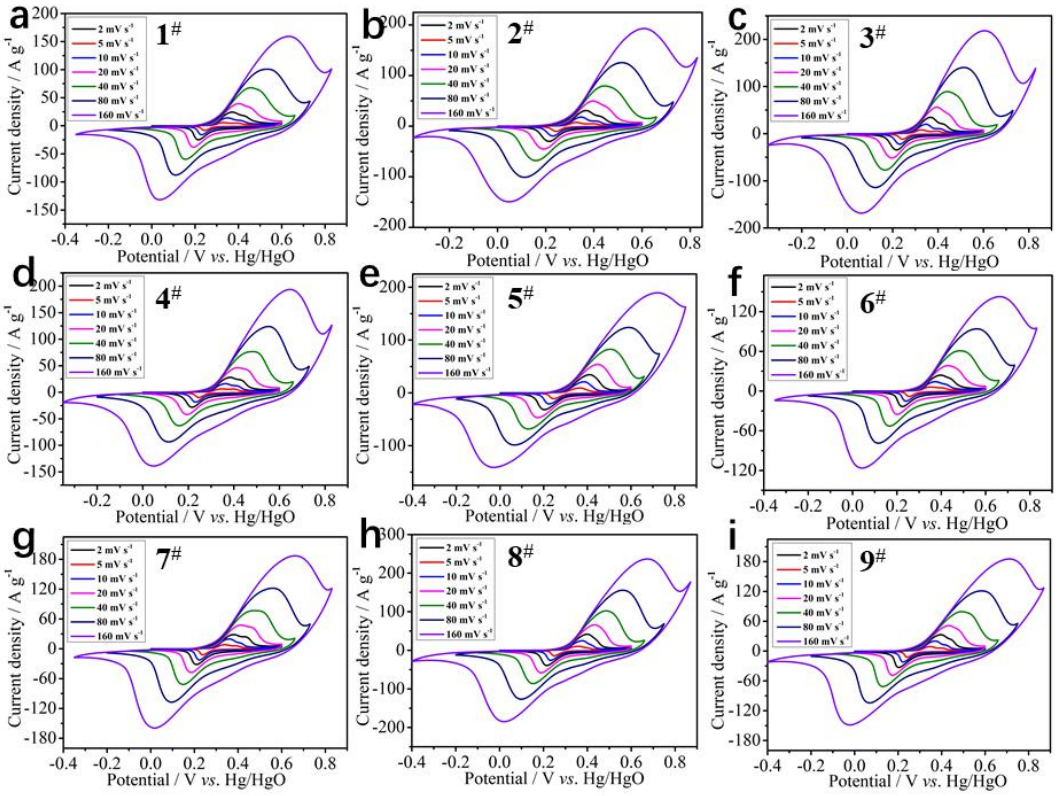

Fig. S2 Performance of single electrode: CV plots at 2-160 mV s^{-1} of $1^{\#}$-$9^{\#}$ samples

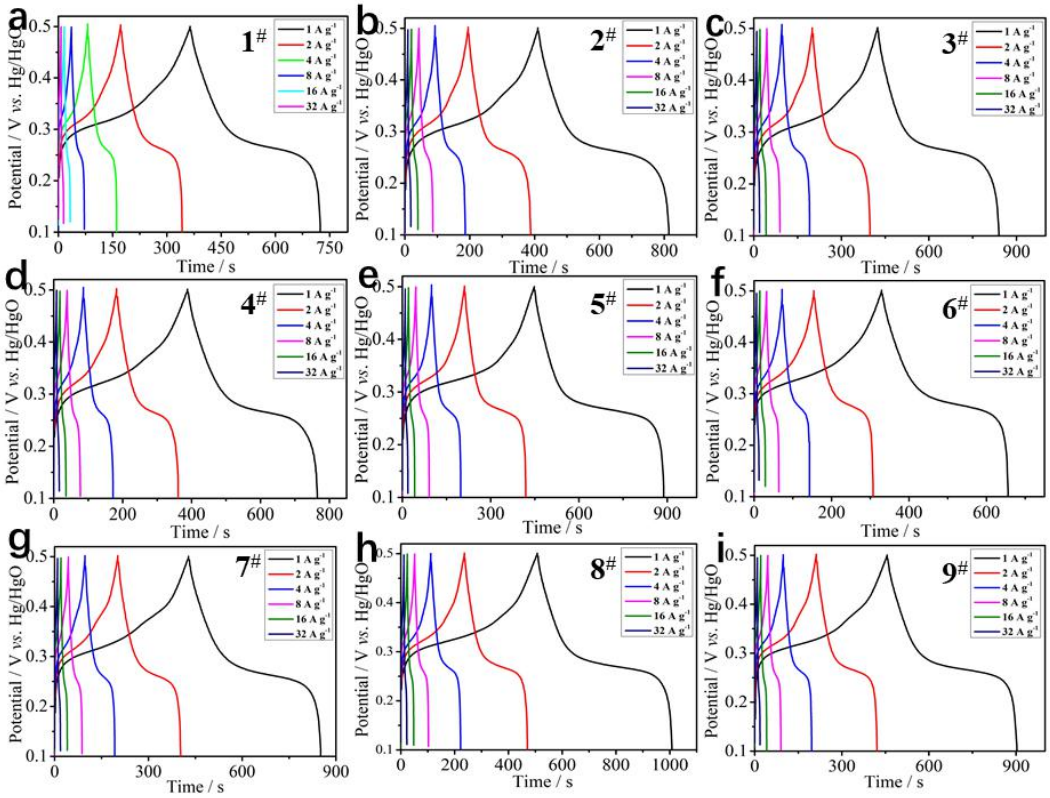

Fig. S3 Performance of single electrode: GCD curves at 1–32 A g^{-1} of $1^{\#}$-$9^{\#}$ samples

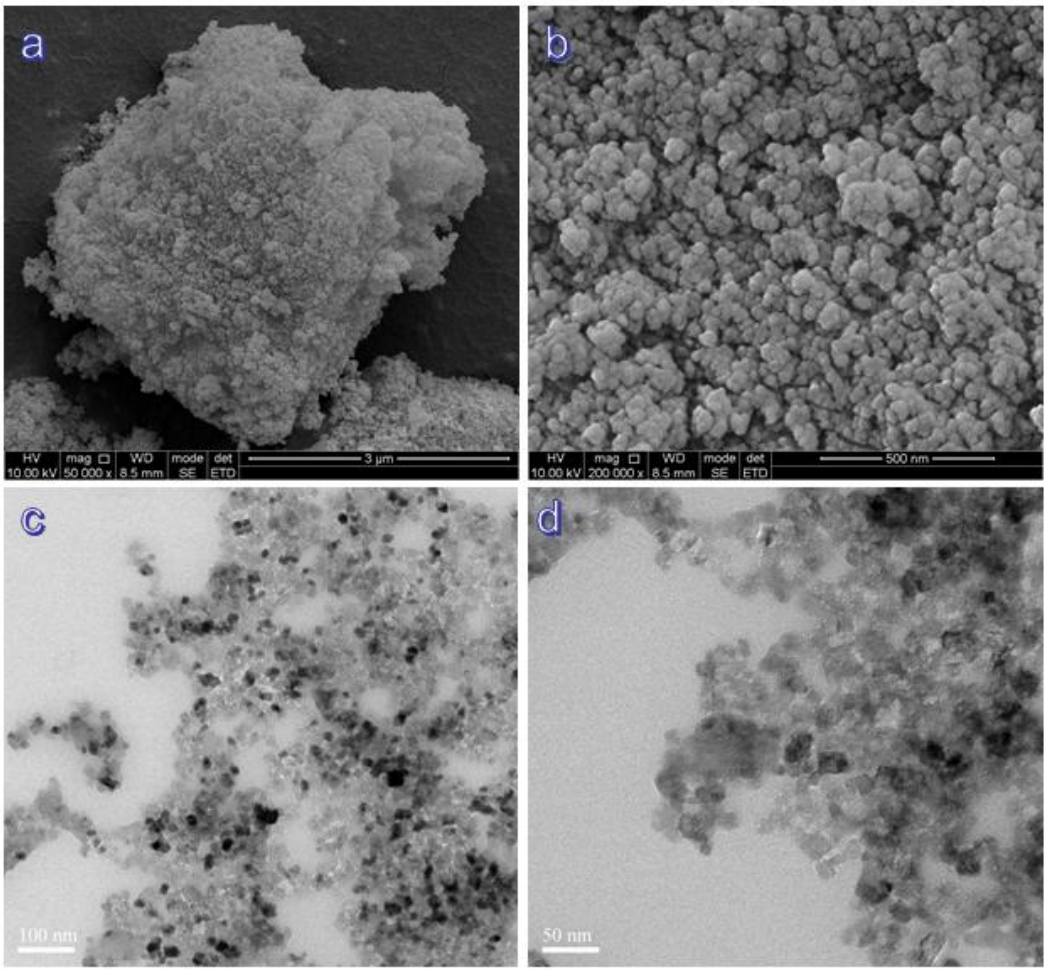

Fig. S4 SEM (a, b) and TEM (c, d) images of the 8# samples

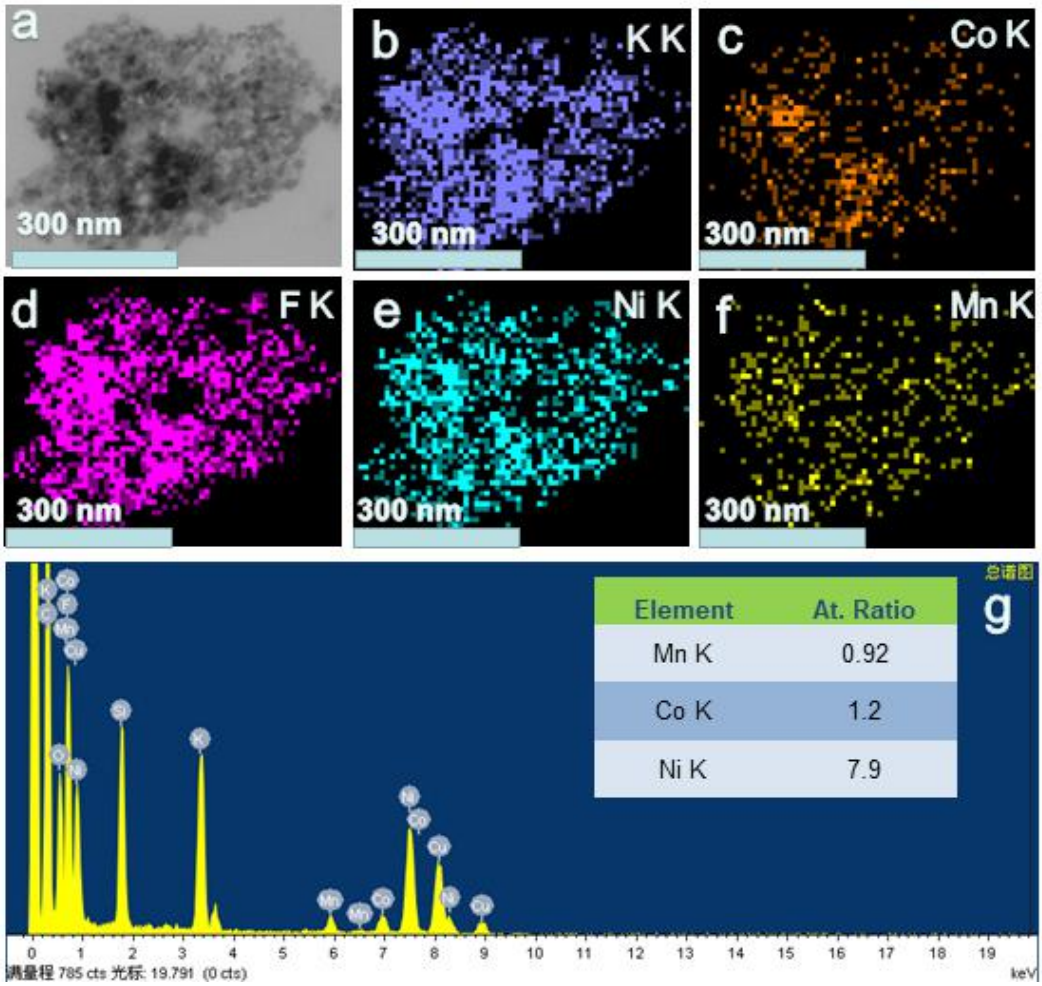

Fig. S5 TEM-mapping (a-f) images and EDS data (g) of the 8# sample.

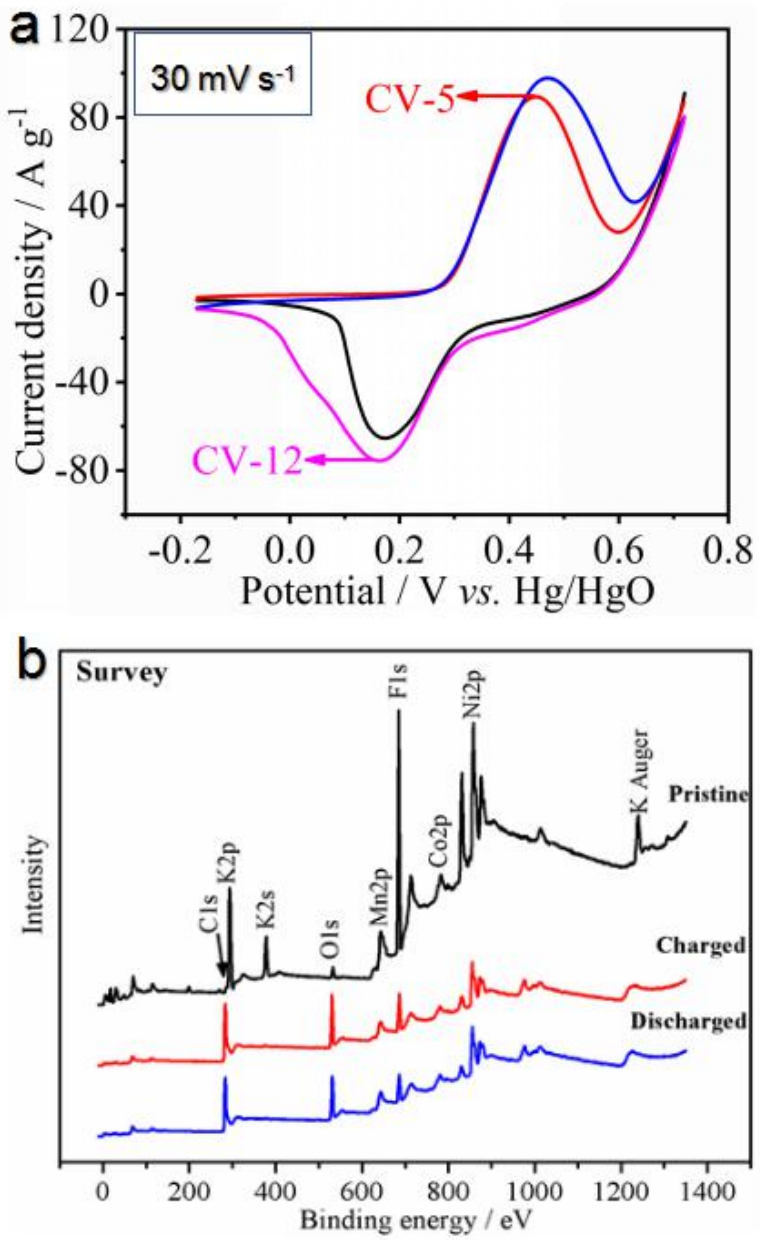

Fig. S6 The typical 5th / 12th segments of CV scans at 30 mV s^{-1} for *ex situ* XPS tests (a) and XPS survey scans in pristine, fully charged and discharged states (after the 5th / 12th segments of CV tests at 30 mV s^{-1}) of the 8$^{\#}$ electrode.

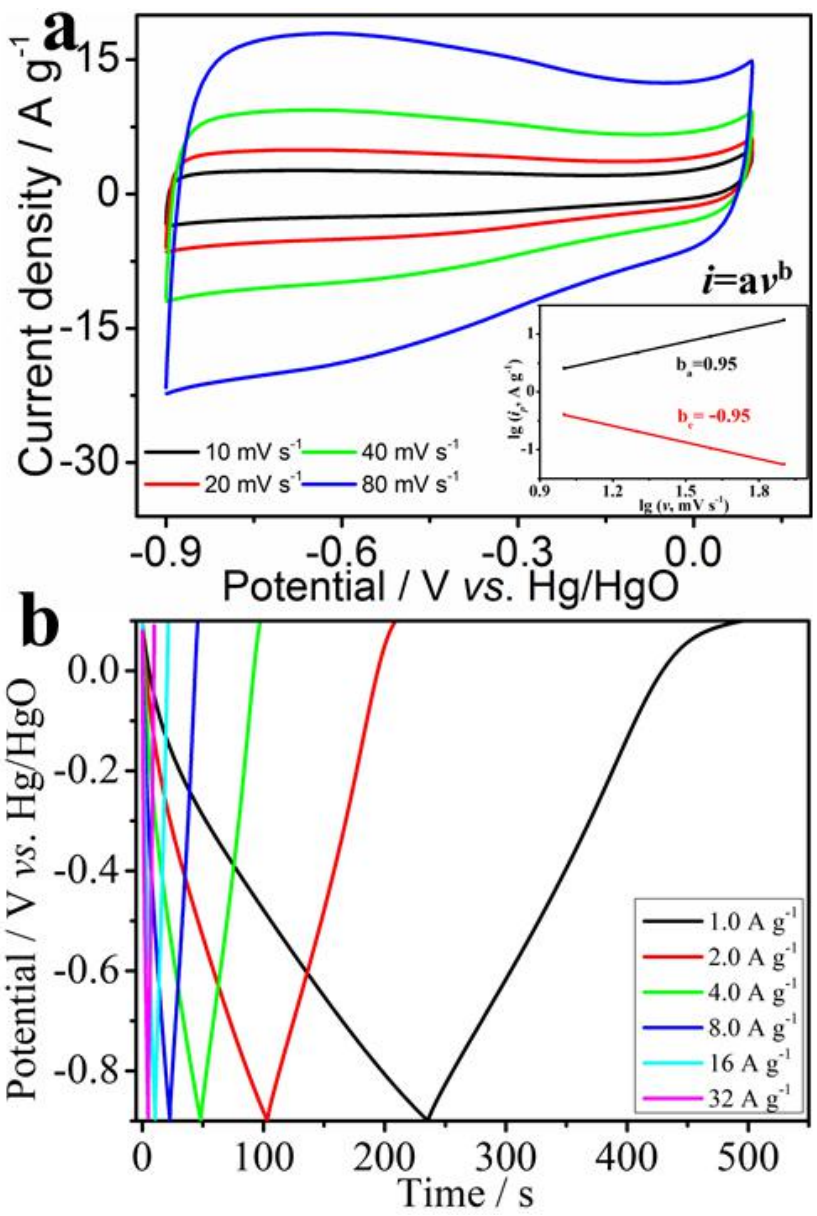

Fig. S7 Performance of AC single electrode: CV plots at 10-80 mV s^{-1} (inset of lg*v*-lg*i*) (a) and GCD curves at 1–32 A g^{-1} (b) of AC electrode.

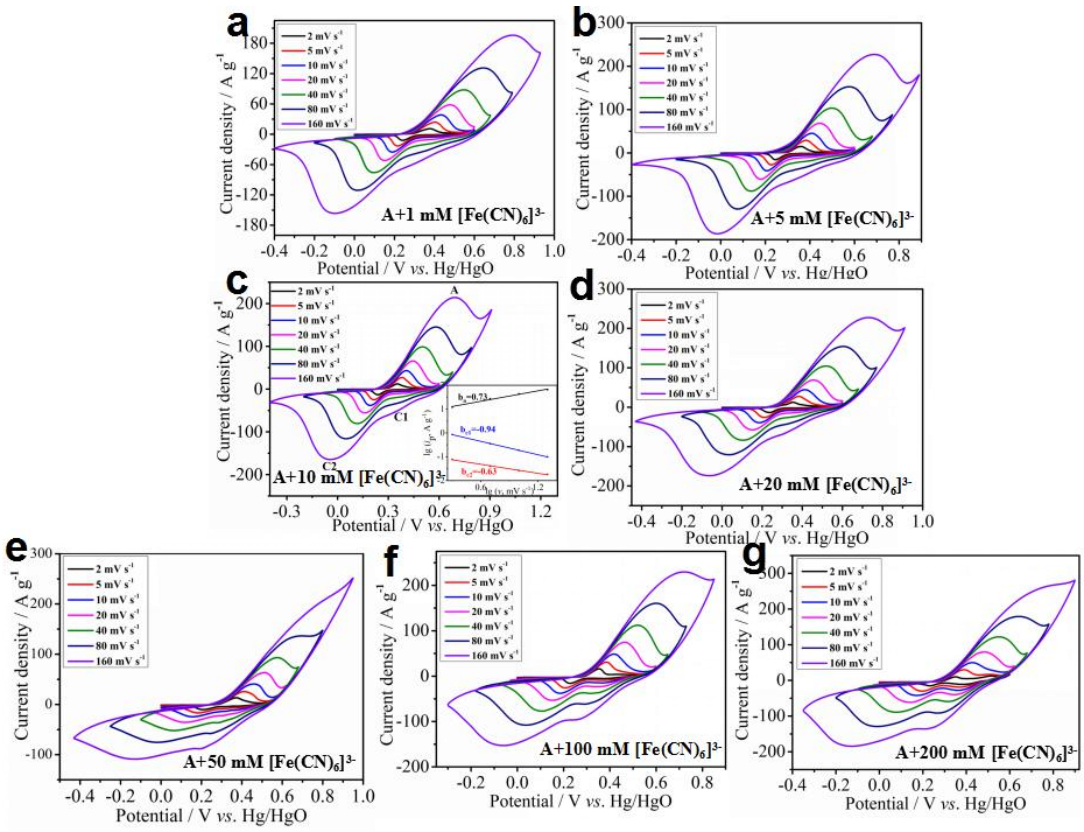

Fig. S8 CV plots at 2-160 mV s^{-1} of the 8# electrode in 3 M KOH+0.5 M LiOH (A) electrolytes with different concentrations of $[Fe(CN)_6]^{3-}$ additive (the inset of **Fig.S8**c shows the plots of lg*v*-lg*i* in A electrolytes and 10 mM $[Fe(CN)_6]^{3-}$ additive.

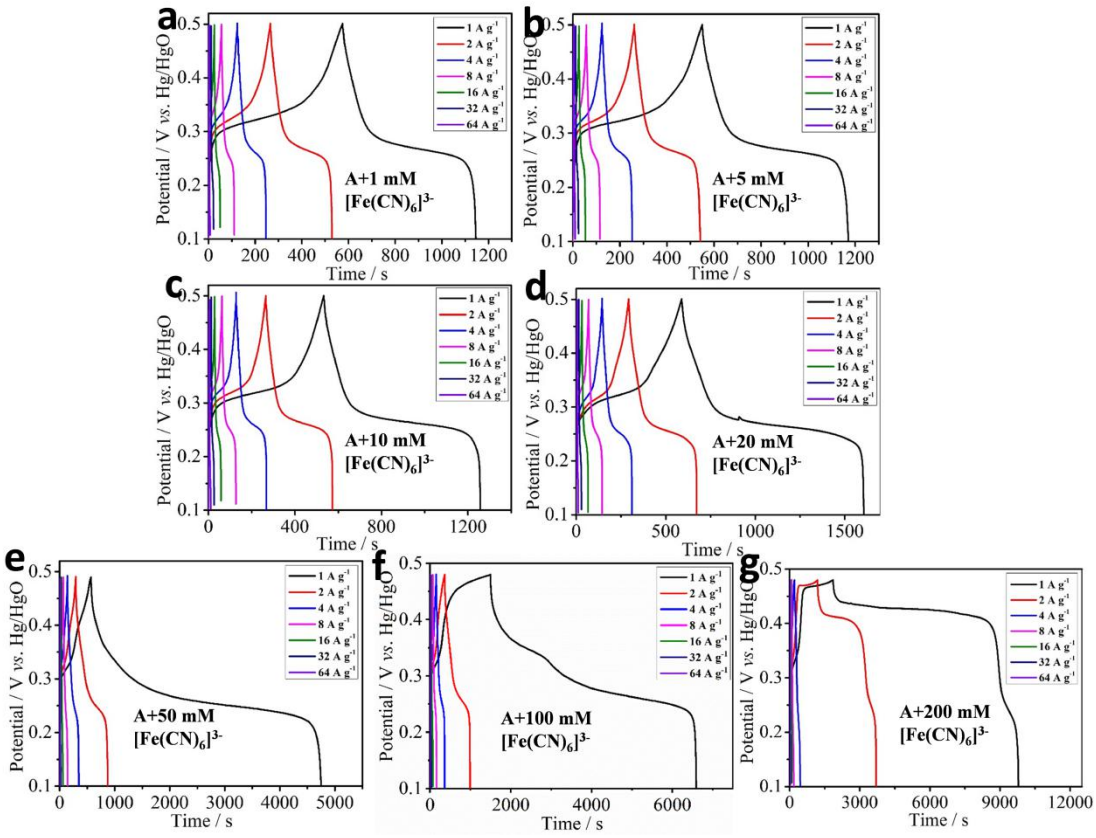

Fig. S9 GCD curves at 1-64 A g^{-1} of the 8# electrode in 3 M KOH+0.5 M LiOH (A) electrolytes with different concentrations of $[Fe(CN)_6]^{3-}$ additives.

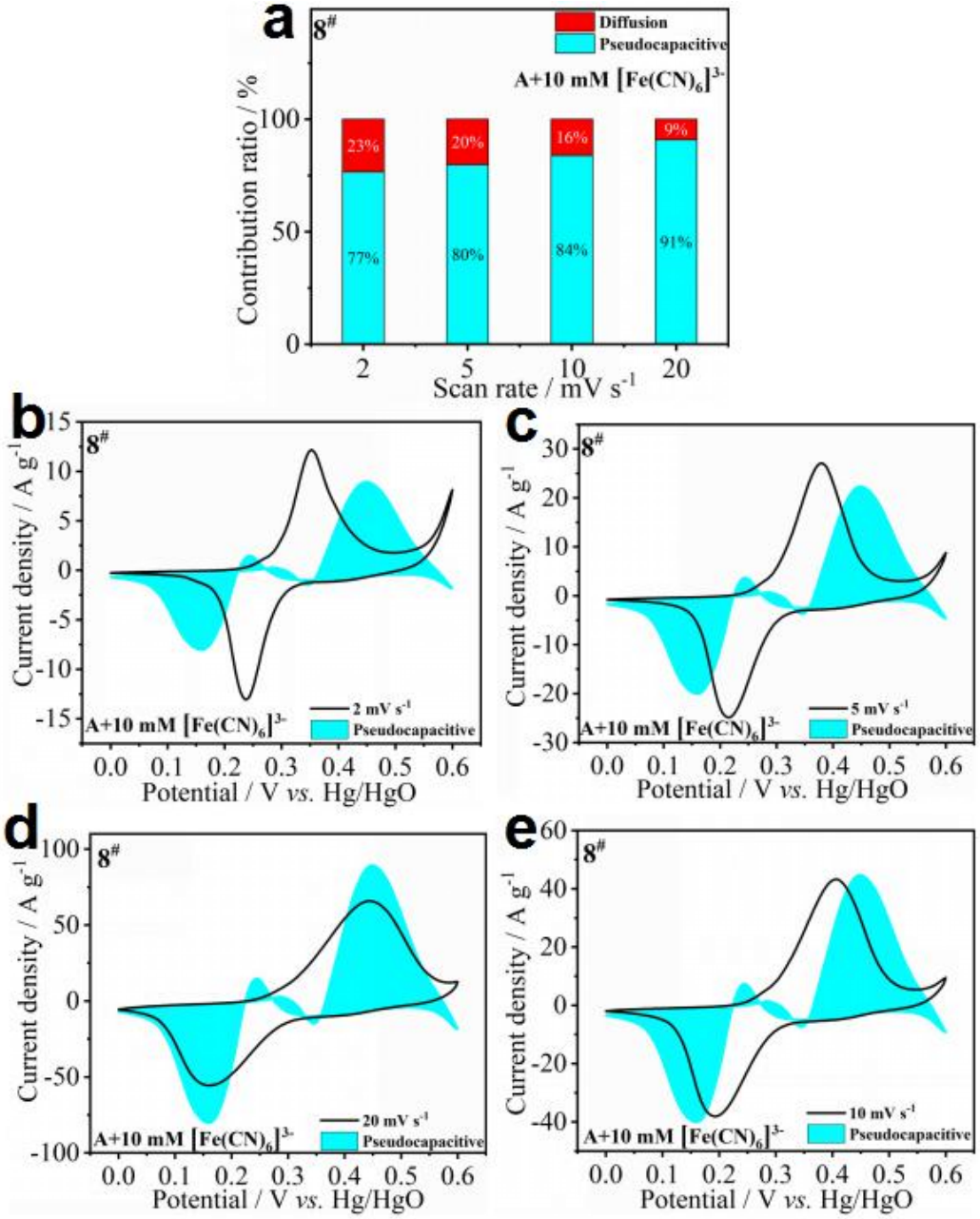

Fig. S10 Pseudocapacitive/diffusion contribution ratio (a) and the area for pseudocapacitive part in the CV plots at 2-20 mV s^{-1} (b-e) of the $8^{\#}$ electrode in 3 M KOH+0.5 M LiOH (A) electrolytes with 10 mM $[Fe(CN)_6]^{3-}$ additives.

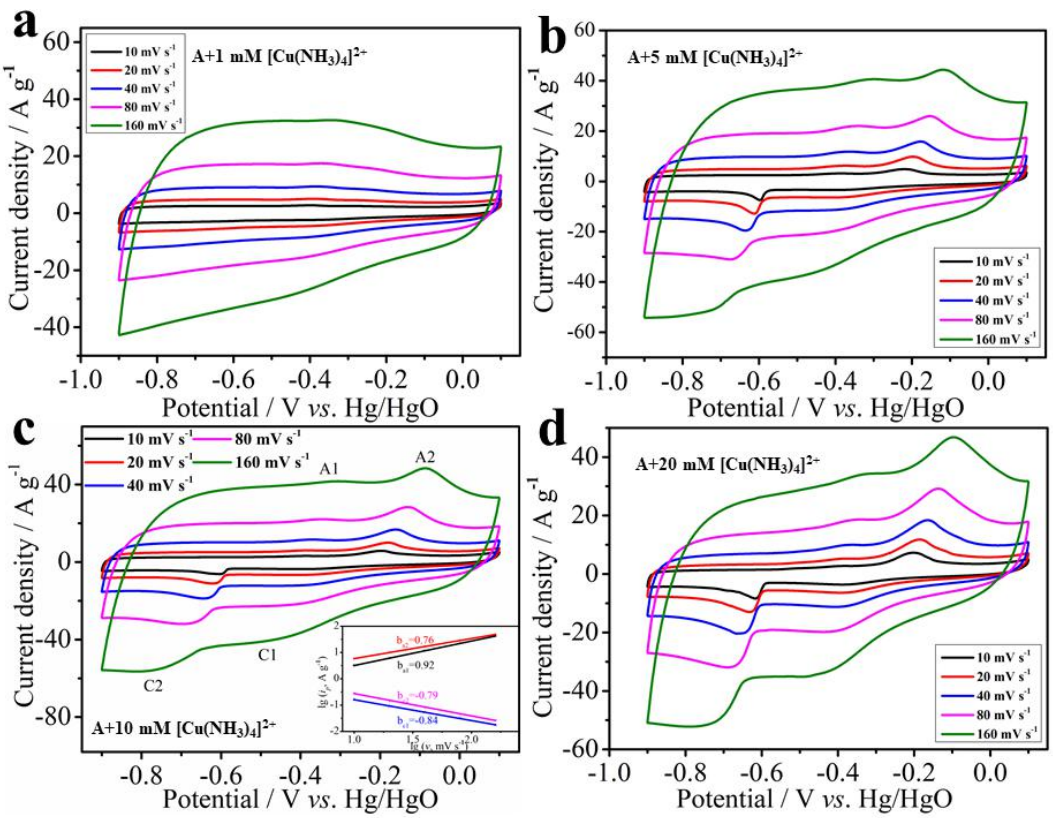

Fig. S11 CV plots at 10-160 mV s^{-1} of the AC electrode in 3 M KOH+0.5 M LiOH (A) electrolytes with different concentrations of $[Cu(NH_3)_4]^{2+}$ additive (the inset of Fig.S10c shows the plots of lg*v*-lg*i* in A+10 mM $[Cu(NH_3)_4]^{2+}$).

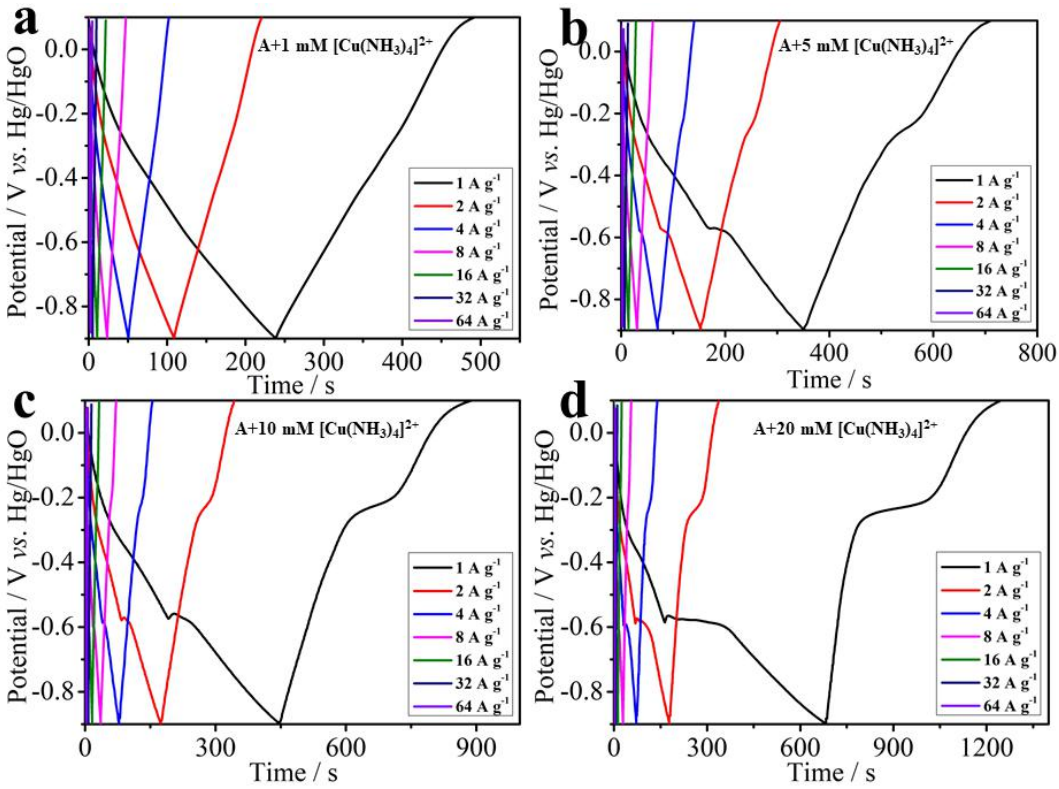

Fig. S12 GCD curves at 1-64 A g^{-1} of the AC electrode in 3 M KOH+0.5 M LiOH (A) with different concentrations of $[Cu(NH_3)_4]^{2+}$ additives.

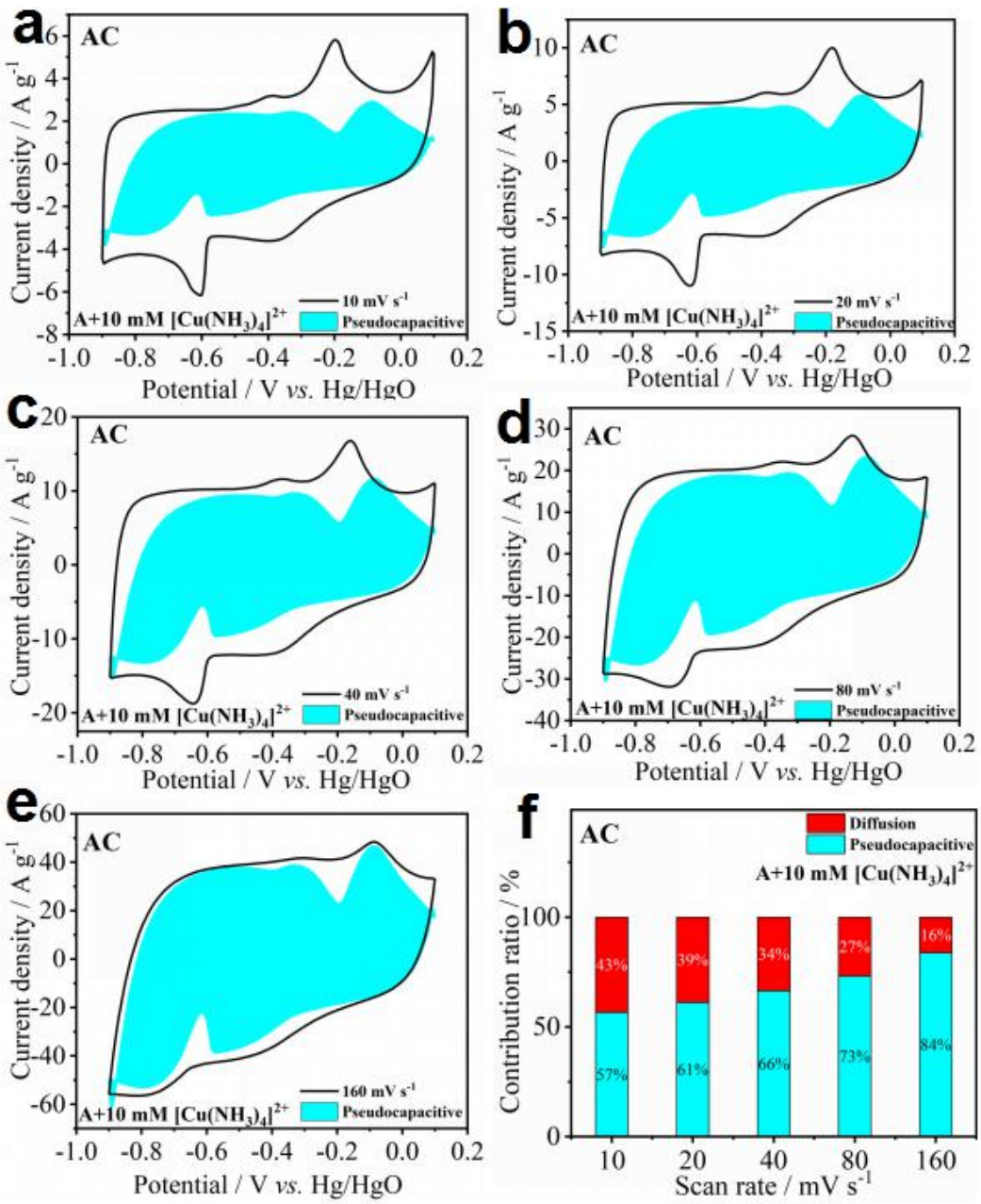

Fig. S13 The area for pseudocapacitive part in the CV plots (a-e) and pseudocapacitive/diffusion contribution ratio (f) at 10-160 mV s^{-1} of the AC electrode in 3 M KOH+0.5 M LiOH (A) electrolytes with10 mM $[Cu(NH_3)_4]^{2+}$ additives.

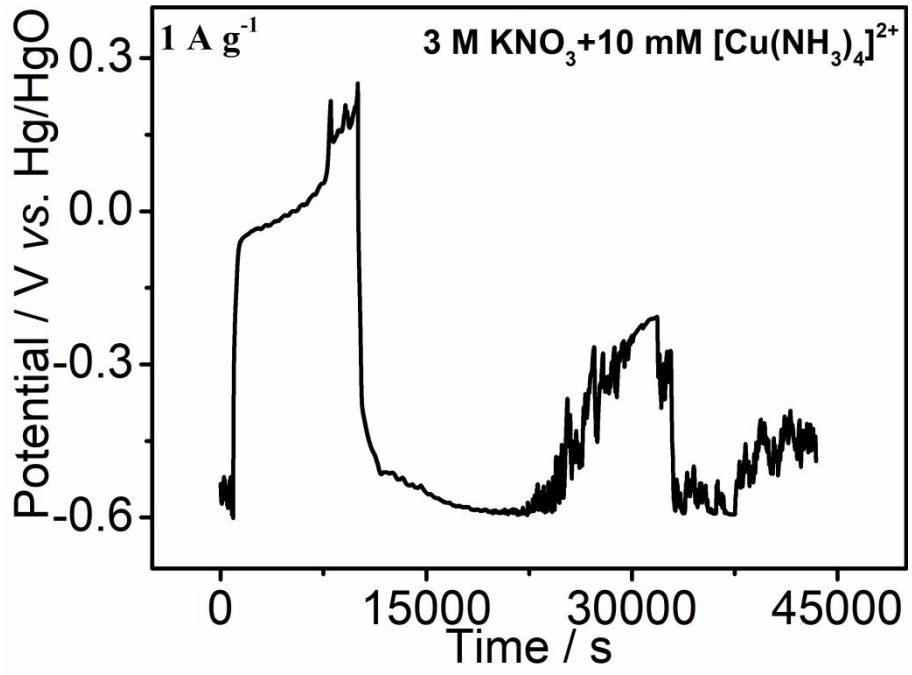

Fig.S14 GCD curves at 1 A g^{-1} of AC electrode in 3 M KNO_3 (C) with 10 mM $[Cu(NH_3)_4]^{2+}$ additive.

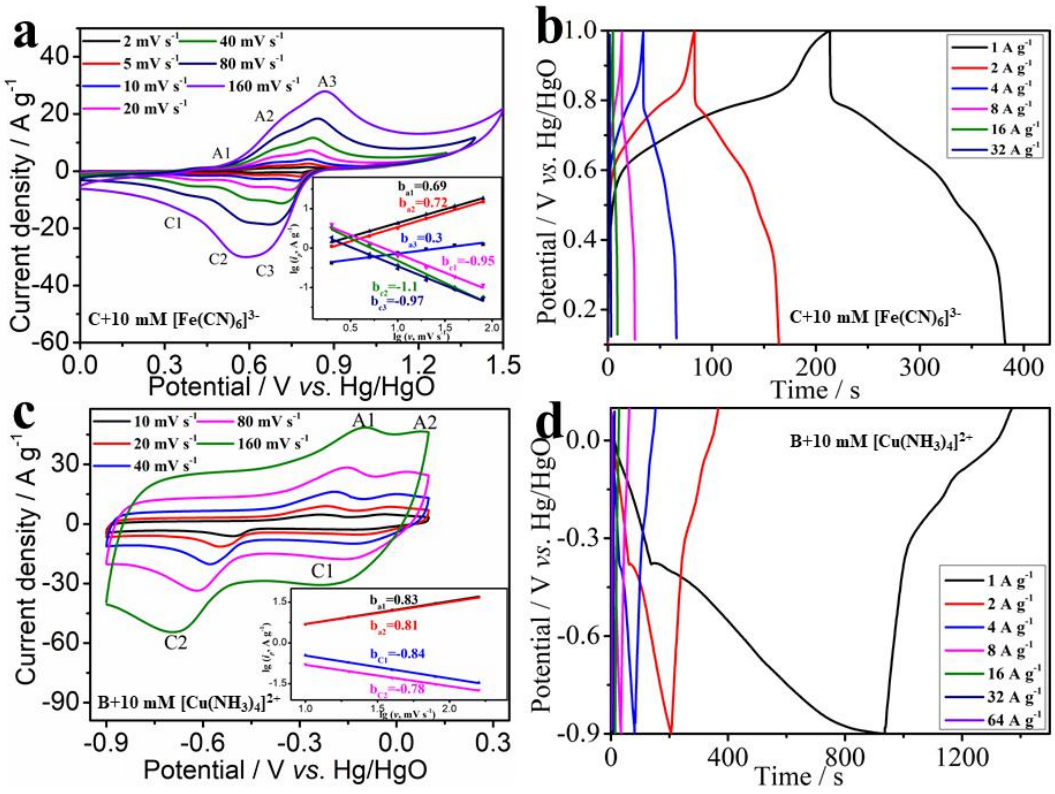

Fig. S15 The CV plots at 2-160 mV s^{-1} (inset shows the plots of lg*v*-lg*i*) (a) and GCD curves at 1-32 A g^{-1} (b) of the 8# electrode in 3 M KNO_3 (C)+10 mM $K_3[Fe(CN)_6]$; the CV plots at 10-160 mV s^{-1} (Inset shows the plots of lg*v*-lg*i*) (c) and GCD curves at 1-64 A g^{-1} (d) of AC electrode in 3 M KCl (B)+10 mM $[Cu(NH_3)_4]^{2+}$.

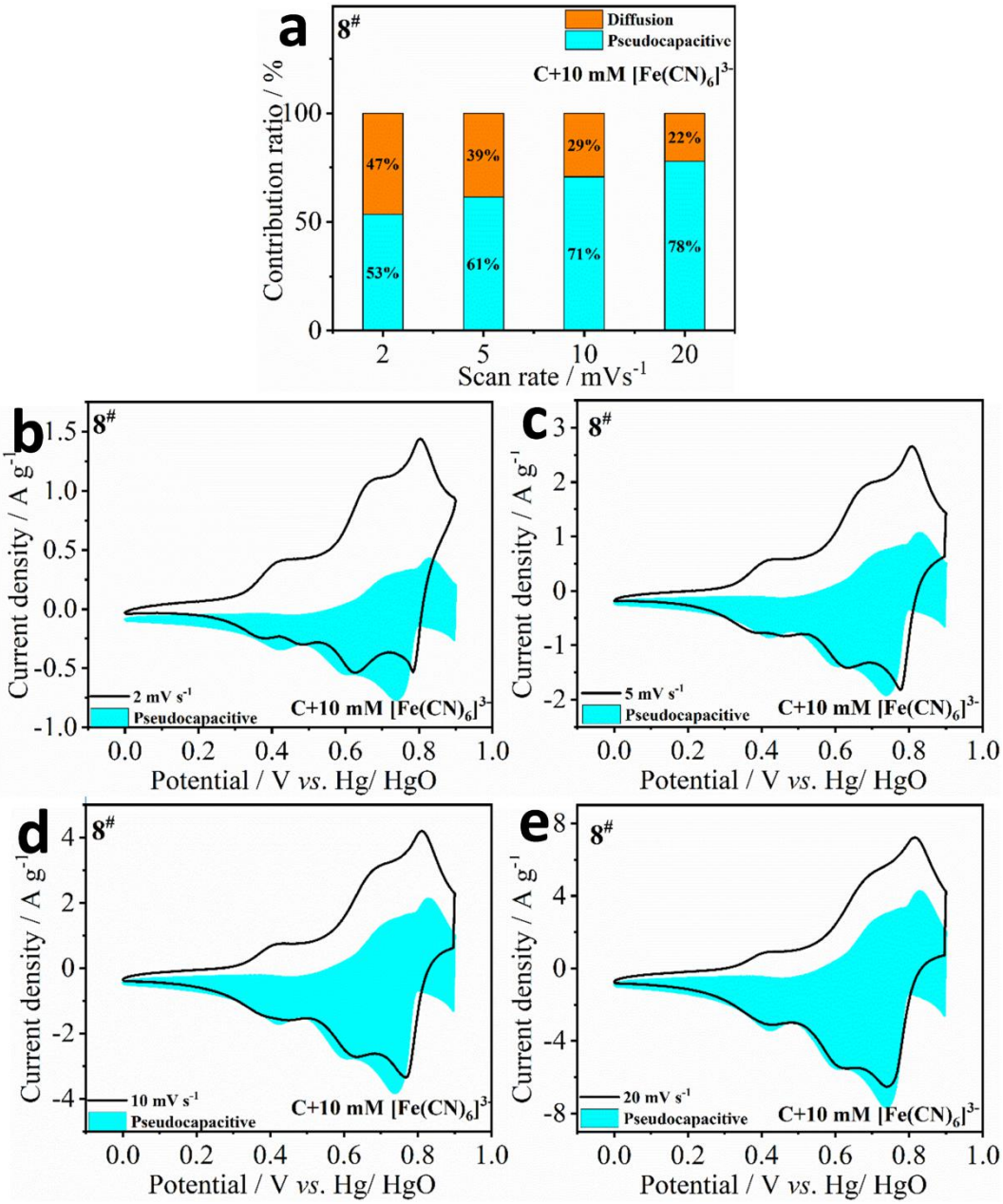

Fig.S16 Pseudocapacitive/diffusion contribution ratio (a) and the area for pseudocapacitive part in the CV plots at 2-20 mV s^{-1} of the $8^{\#}$ electrode in 3 M KNO_3 (C) electrolytes with 10 mM $[Fe(CN)_6]^{3-}$ additives.

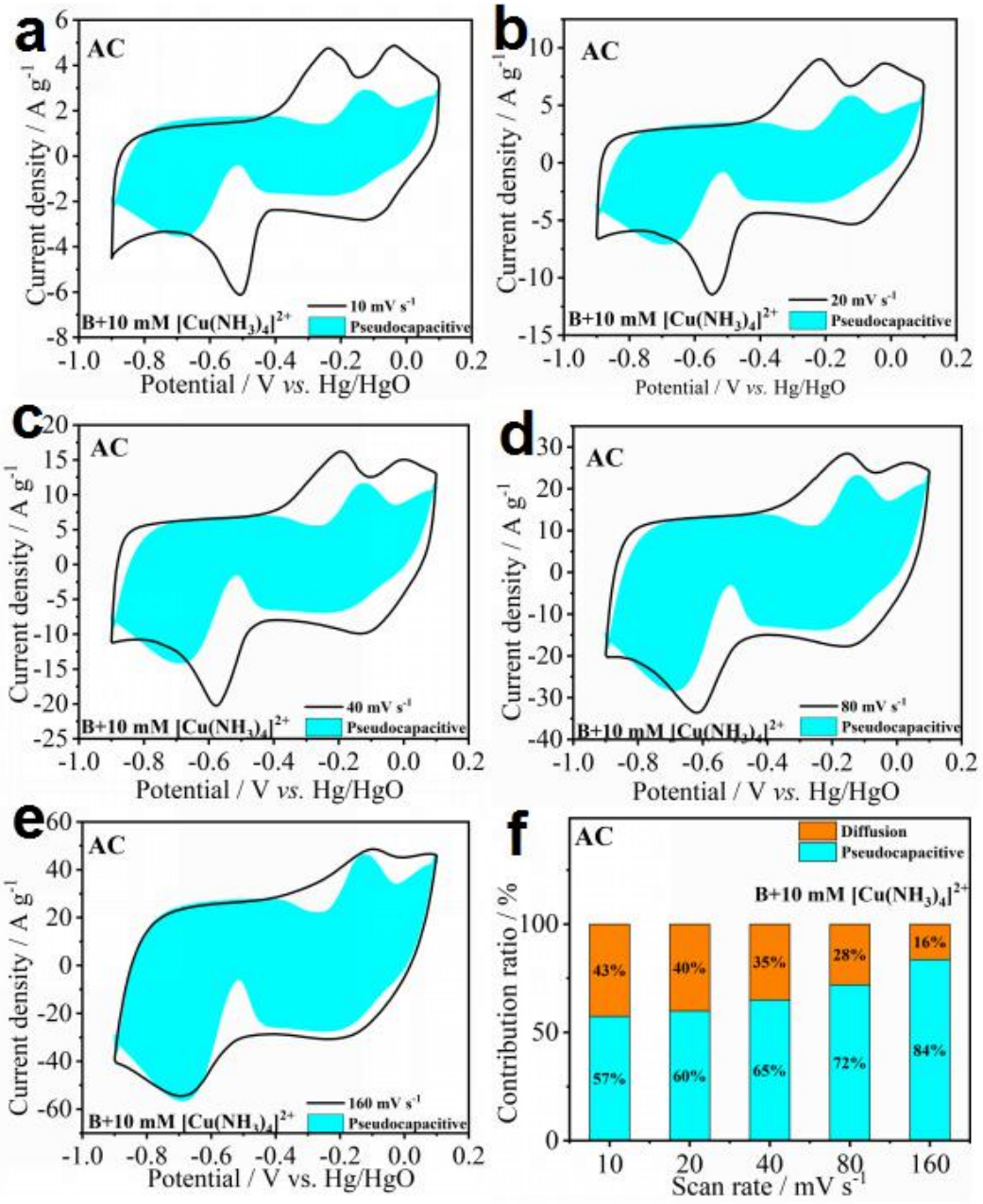

Fig.S17 The area for pseudocapacitive part in the CV plots (a-e) and pseudocapacitive/diffusion contribution ratio (f) at 10-160 mV s^{-1} of the AC electrode in 3 M KCl (B) electrolytes with10 mM $[Cu(NH_3)_4]^{2+}$ additives.

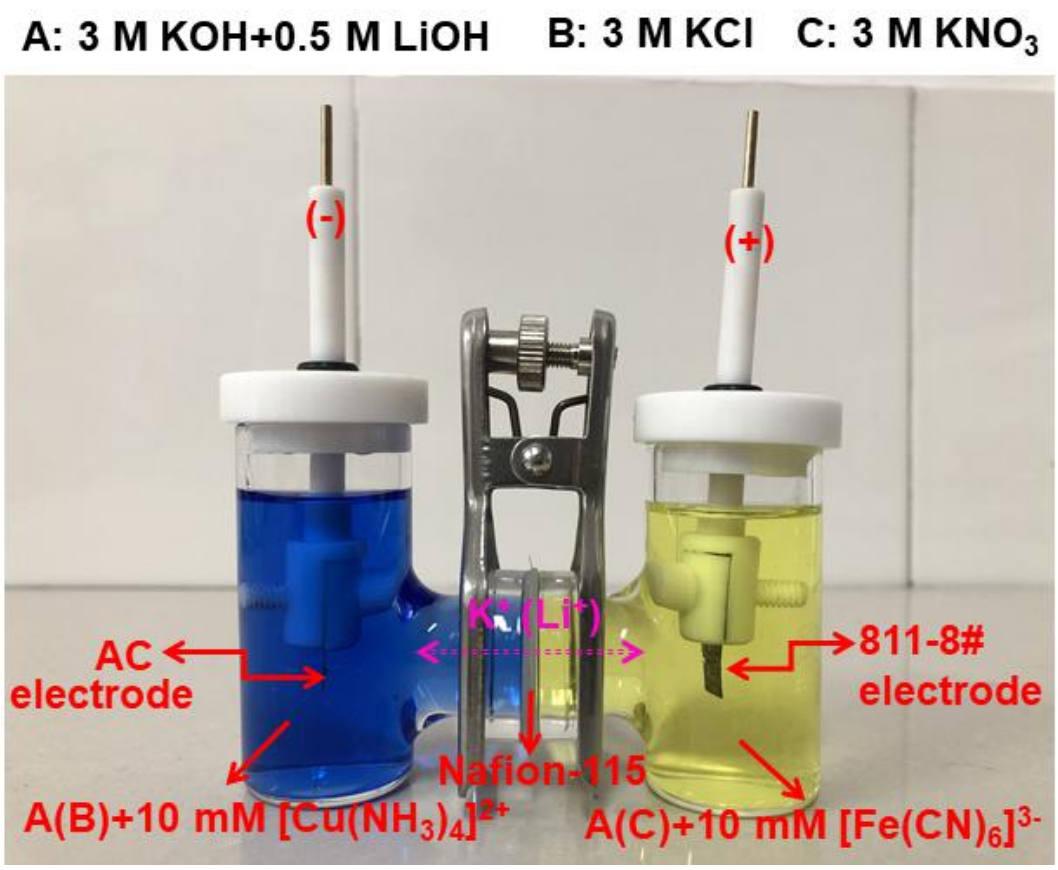

Fig. S18 The detail drawing for H-type SC structure

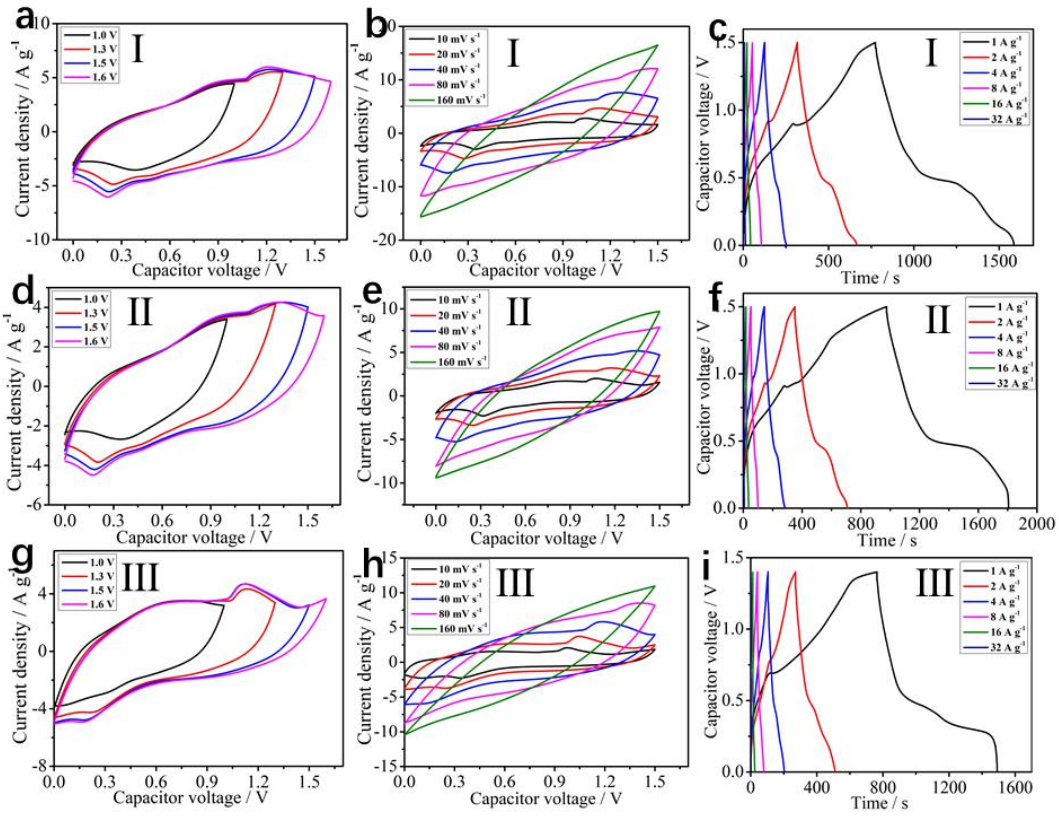

Fig. S19 The CV window (a, d, g), CV plots of 10-160 mV s^{-1} (b, e, h) and GCD curves at 1–32 A g^{-1} (c, f, i) of Ⅰ, Ⅱ and Ⅲ H-type capacitors

Ⅰ: AC (A+10 mM $[Cu(NH_3)_4]^{2+}$) //811-8# (A+10 mM $[Fe(CN)_6]^{3-}$)

Ⅱ: AC (A+10 mM $[Cu(NH_3)_4]^{2+}$) // 811-8# (A+20 mM $[Fe(CN)_6]^{3-}$)

Ⅲ: AC (B+10 mM $[Cu(NH_3)_4]^{2+}$) // 811-8# (A+10 mM $[Fe(CN)_6]^{3-}$)

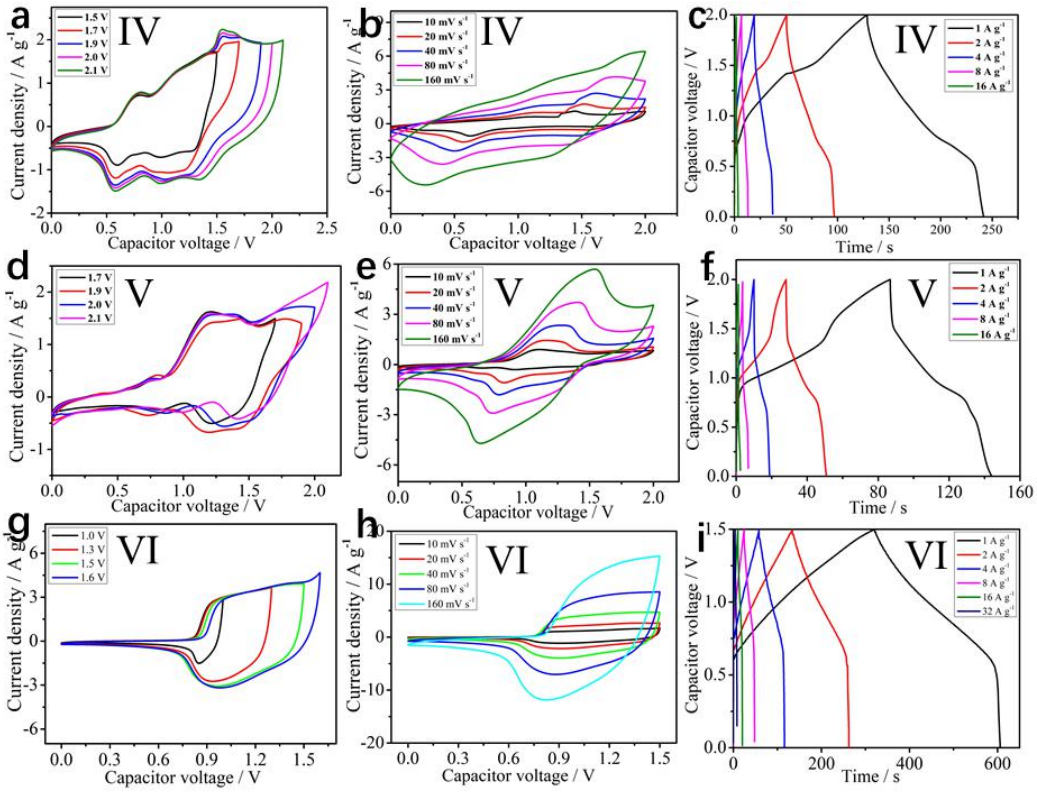

Fig. S20 The CV window (a, d, g), CV plots of 10-160 mV s^{-1} (b, e, h) and GCD curves at 1–32 A g^{-1} (c, f, i) of Ⅳ, Ⅴ and Ⅵ H-type capacitors

Ⅳ: AC (A+10 mM $[Cu(NH_3)_4]^{2+}$) // 811-8# (C+10 mM $[Fe(CN)_6]^{3-}$)

Ⅴ: AC (B+10 mM $[Cu(NH_3)_4]^{2+}$) // 811-8# (C+10 mM $[Fe(CN)_6]^{3-}$)

Ⅵ: AC (A) // 811-8# (A)

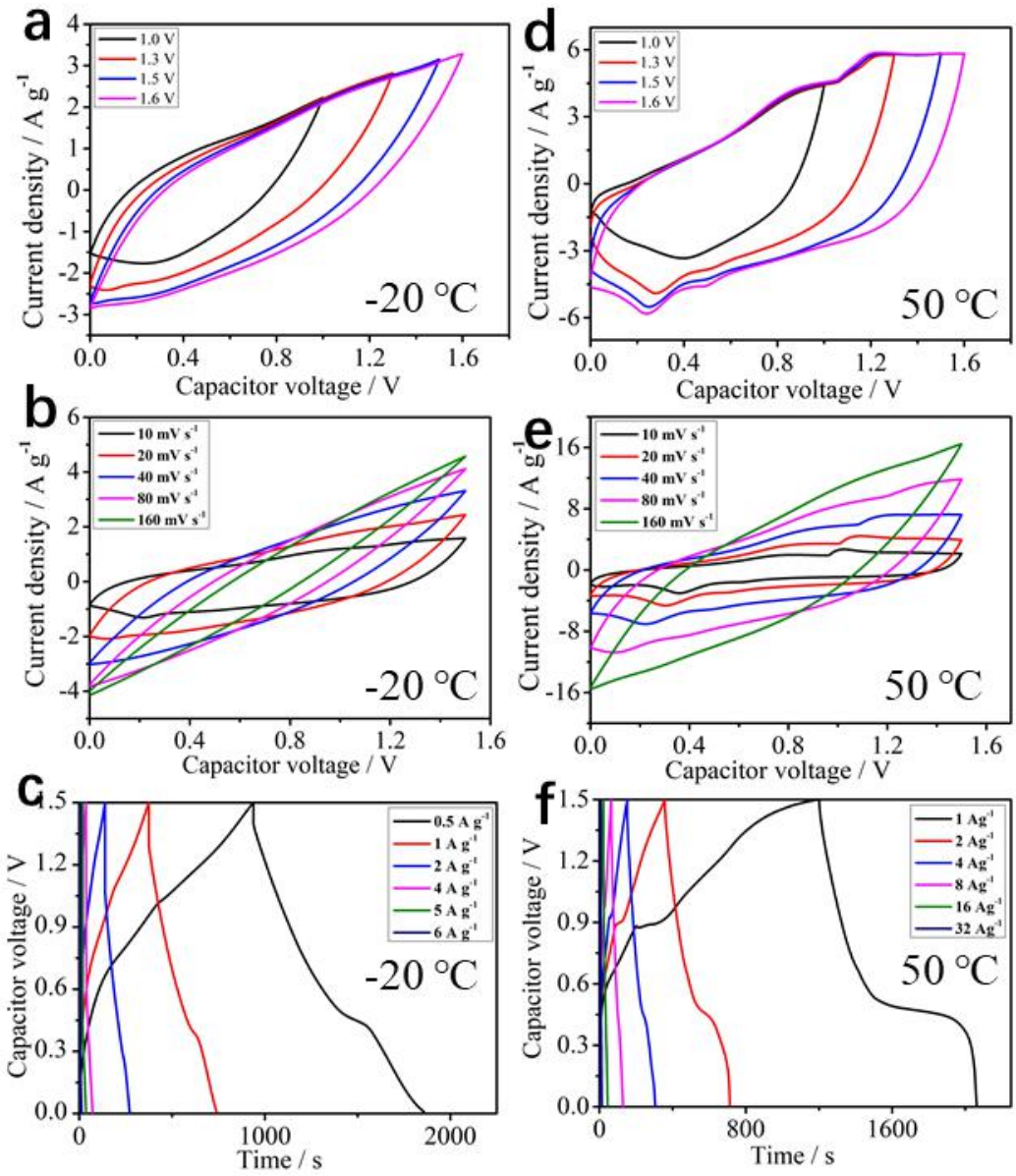

Fig. S21 The CV window (a, d), CV plots of 10-160 mV s^{-1} (b, e) and GCD curves at 1–32 A g^{-1} (c, f) of Ⅰ H-type capacitor with high and low temperatures.

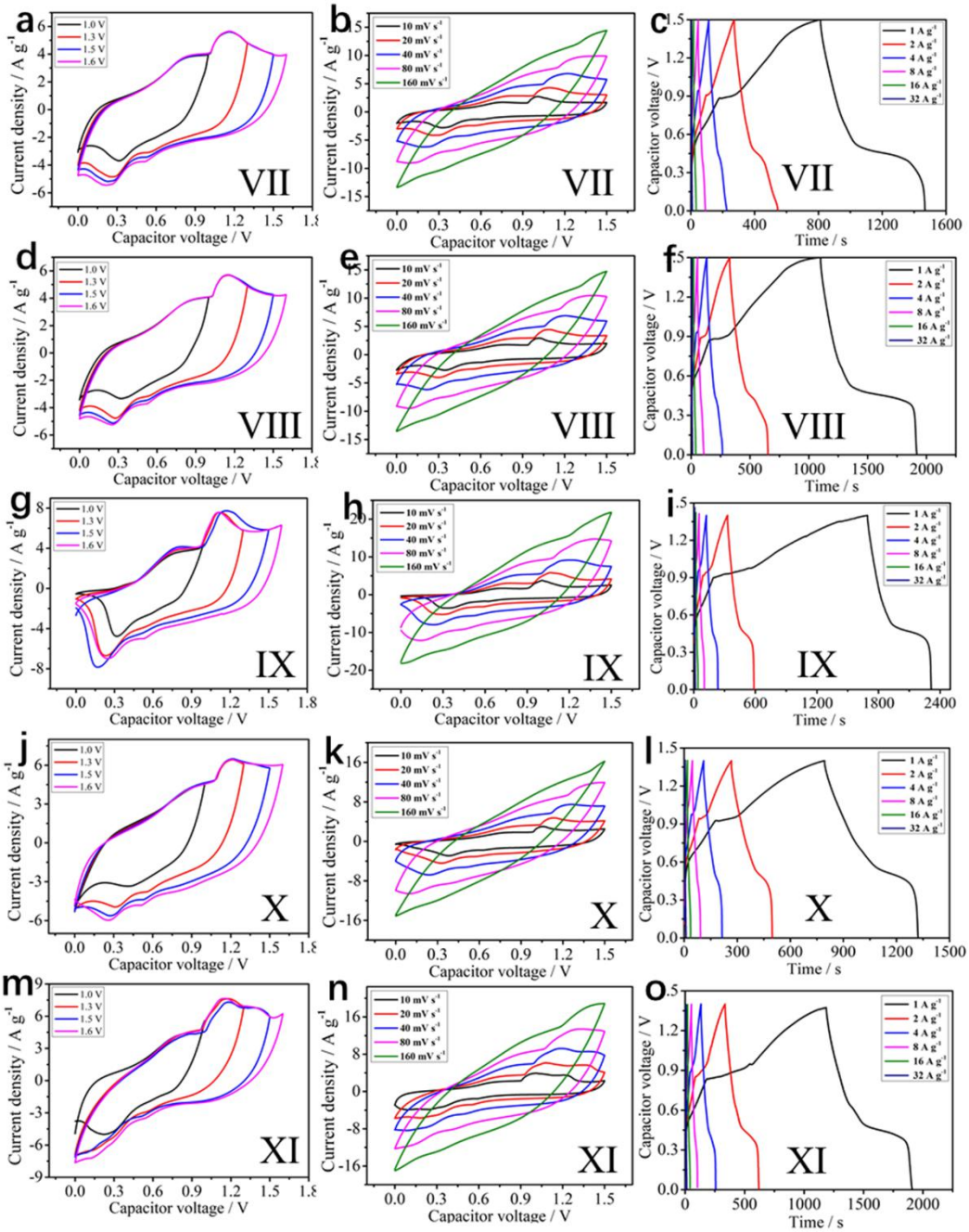

Fig. S22 The CV window (a, d, g, j, m), CV plots of 10-160 mV s^{-1} (b, e, h, k, n) and GCD curves at 1–32 A g^{-1} (c, f, i, l, o) of Ⅶ-Ⅺ H-type capacitors under high temperature.

Ⅶ: AC (A+10 mM $[Cu(NH_3)_4]^{2+}$) // 811-8# (A+10 mM $[Fe(CN)_6]^{3-}$+0.5% Na_2MoO_4)

Ⅷ: AC (A+10 mM $[Cu(NH_3)_4]^{2+}$) // 811-8# (A+10 mM $[Fe(CN)_6]^{3-}$+1.0% Na_2MoO_4)

Ⅸ: AC (A+10 mM $[Cu(NH_3)_4]^{2+}$) //811-8# (A+10 mM $[Fe(CN)_6]^{3-}$+1.5% Na_2MoO_4)

Ⅹ: AC (A+10 mM $[Cu(NH_3)_4]^{2+}$) // 811-8# (A′+10 mM $[Fe(CN)_6]^{3-}$+1.0% Na_2MoO_4)

Ⅺ: AC (A+10 mM $[Cu(NH_3)_4]^{2+}$) // 811-8# (A″+10 mM $[Fe(CN)_6]^{3-}$+1.0% Na_2MoO_4)

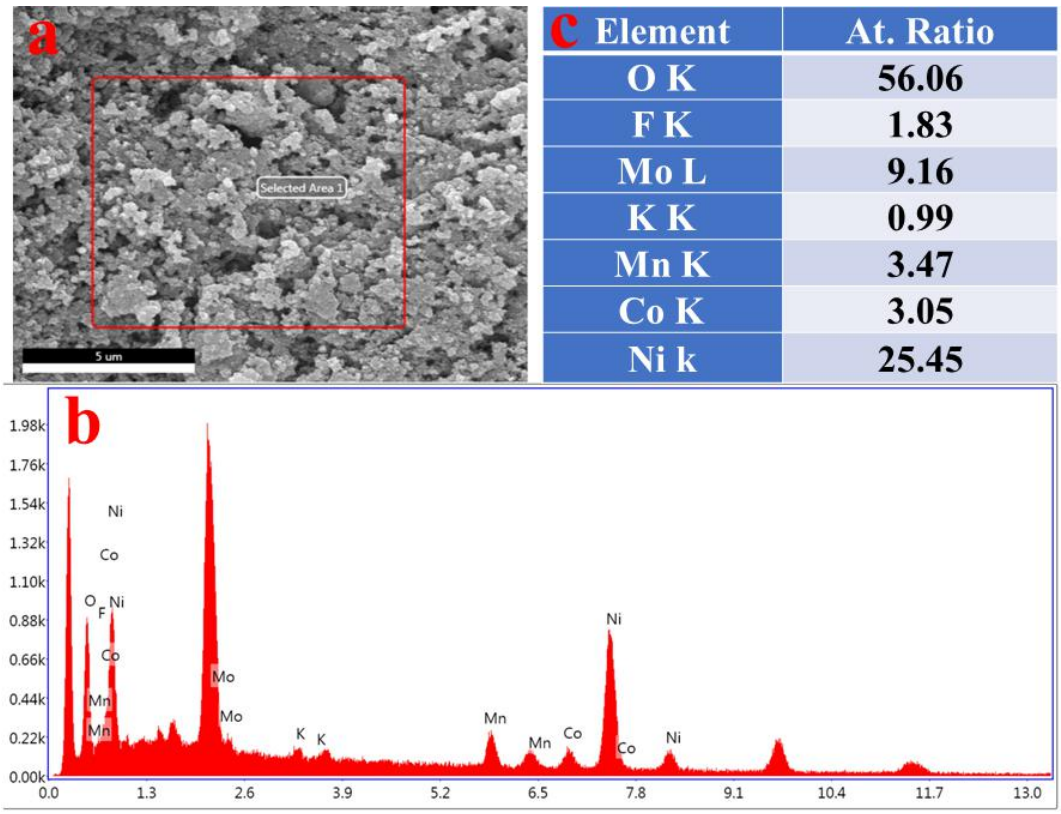

Fig. S23 The EDS data of the 8# cathode in the Ⅷ H-type capacitor [AC (A+10 mM $[Cu(NH_3)_4]^{2+}$) // 811-8$^{\#}$ (A+10 mM $[Fe(CN)_6]^{3-}$+1.0% Na_2MoO_4)] after the cycling tests under high temperature.

Table S1 The orthogonal analysis of KNCMF-811($1^{\#}$-$9^{\#}$) electrodes in A electrolytes

Samples		Experimental factors				Experimental data		
		A	B	C	D	Specific capacity (C g^{-1})	Rate (%)	Cycle retention (%)
$1^{\#}$		A1	B1	C1	D1	360	64	73
$2^{\#}$		A1	B2	C2	D2	404	72.9	64
$3^{\#}$		A1	B3	C3	D3	416	70.8	63
$4^{\#}$		A2	B1	C2	D3	377	66.9	48
$5^{\#}$		A2	B2	C3	D1	440	67	47
$6^{\#}$		A2	B3	C1	D2	327	60.9	59
$7^{\#}$		A3	B1	C3	D2	423	70.7	67
$8^{\#}$		A3	B2	C1	D3	501	71	62
$9^{\#}$		A3	B3	C2	D1	447	65.1	44
Specific capacitance	K1	1180	1160	1188	1247			
	K2	1144	1345	1228	1154			
	K3	1371	1190	1279	1294			
	k1	393.3	386.7	396	415.7			
	k2	381.3	448.3	409.3	384.7			
	k3	457	396.7	426.3	431.3			
	Range	75.7	61.6	30.3	46.6			
Rate (%)	K1	207.7	201.6	195.9	196.1			
	K2	194.8	210.9	204.9	204.5			
	K3	206.8	196.8	208.5	208.7			
	k1	69.2	67.2	65.3	65.37			
	k2	64.9	70.3	68.3	68.17			
	k3	68.9	65.6	69.5	69.57			
	Range	4.3	4.7	4.2	4.2			
Cycle retention (%)	K1	200.0	188.0	194.0	164.0			
	K2	154.0	173.0	156.0	190.0			
	K3	173.0	166.0	177.0	173.0			
	k1	66.7	62.7	64.7	54.7			
	k2	51.3	57.7	52.0	63.3			
	k3	57.7	55.3	59.0	57.7			
	Range	15.4	7.4	12.7	8.6			
Optimal experimental condition						A3B2C1D3 ($8^{\#}$)		

A: n(total metal salt):n(KF), A1 = 1:2, A2 = 1:2.5, A3 = 1:3.

B: Solvent, B1 = EG+EA (1:1), B2 = EG+NPA (1:1), B3 = EG+NBA (1:1), Total volume=36 mL.

C: Temperature, C1 = 160 ℃, C2 = 170 ℃, C3 = 180 ℃.

D: Time, D1 = 6 h, D2 = 12 h, D3 = 24 h.

Table S2 Specific capacity (C g^{-1}) and cycling retention (%) of the KNCMF-811 ($1^{\#}$-$9^{\#}$) and AC electrodes in A electrolytes

Samples	Current density/（A g^{-1}）						Cycling Retention % / 8 A g^{-1} /10000 cycles
	1	2	4	8	16	32	
$1^{\#}$	360	340	320	286.4	259.2	230.4	73
$2^{\#}$	404	386	372	343.2	320.4	294.4	64
$3^{\#}$	416	396	380	344	321.9	294.7	63
$4^{\#}$	377	358	344	315.2	281.9	252.2	48
$5^{\#}$	440	416	396	365.6	324.8	294.7	47
$6^{\#}$	327	306	284	254.4	230.6	199	59
$7^{\#}$	423	402	380	349.6	326.7	299.2	67
$8^{\#}$	501	468	444	411.2	381.8	355.8	62
$9^{\#}$	447	418	392	363.3	321.3	291.2	44
AC	260	211.6	195.6	183.2	172.8	160	95

Table S3. EIS fitting parameters of the 8# electrode before and after cycling test in A electrolytes.

	Model	L (H)	R_{ESR} (Ω)	C (F)	R_{ct} (Ω)	W (S $sec^{0.5}$)	C (F)	χ^2
Before CT	*LR(C(RW))C*	9.8×10^{-7}	0.62	1.7×10^{-3}	0.53	0.32	0.64	5.8×10^{-3}
After CT		8.2×10^{-7}	0.73	8.1×10^{-4}	1.03	0.055	0.23	4.6×10^{-3}

Table S4 The preparation of specific electrolytes

Electrolytes	Supporting electrolytes	Additive
A	9.9018 g KOH+1.1042 g LiOH•H_2O	-
A+1 mM $[Fe(CN)_6]^{3-}$	9.9018 g KOH+1.1042 g LiOH•H_2O	0.0165 g $K_3[Fe(CN)_6]$
A+5 mM $[Fe(CN)_6]^{3-}$	9.9018 g KOH+1.1042 g LiOH•H_2O	0.0827 g $K_3[Fe(CN)_6]$
A+10 mM $[Fe(CN)_6]^{3-}$	9.9018 g KOH+1.1042 g LiOH•H_2O	0.1655 g $K_3[Fe(CN)_6]$
A+20 mM $[Fe(CN)_6]^{3-}$	9.9018 g KOH+1.1042 g LiOH•H_2O	0.3309 g $K_3[Fe(CN)_6]$
A+50 mM $[Fe(CN)_6]^{3-}$	9.9018 g KOH+1.1042 g LiOH•H_2O	0.8273 g $K_3[Fe(CN)_6]$
A+100 mM $[Fe(CN)_6]^{3-}$	9.9018 g KOH+1.1042 g LiOH•H_2O	1.6545 g $K_3[Fe(CN)_6]$
A+200 mM $[Fe(CN)_6]^{3-}$	9.9018 g KOH+1.1042 g LiOH•H_2O	3.3090 g $K_3[Fe(CN)_6]$
A+1 mM $[Cu(NH_3)_4]^{2+}$	9.9018 g KOH+1.1042 g LiOH•H_2O	0.0126 g $CuSO_4$•$5H_2O$ +0.1 mL NH_3•H_2O
A+5 mM $[Cu(NH_3)_4]^{2+}$	9.9018 g KOH+1.1042 g LiOH•H_2O	0.0631 g $CuSO_4$•$5H_2O$ +0.5 mL NH_3•H_2O
A+10 mM $[Cu(NH_3)_4]^{2+}$	9.9018 g KOH+1.1042 g LiOH•H_2O	0.1261 g $CuSO_4$•$5H_2O$ +1 mL NH_3•H_2O
A+20 mM $[Cu(NH_3)_4]^{2+}$	9.9018 g KOH+1.1042 g LiOH•H_2O	0.2522 g $CuSO_4$•$5H_2O$ +2 mL NH_3•H_2O
C+10 mM $[Fe(CN)_6]^{3-}$	15.3182 g KNO_3	0.1655 g $K_3[Fe(CN)_6]$
B+10 mM $[Cu(NH_3)_4]^{2+}$	11.2387 g KCl	0.1261 g $CuSO_4$•$5H_2O$ +1 mL NH_3•H_2O
A+10 mM $[Fe(CN)_6]^{3-}$+0.5 wt% Na_2MoO_4	9.9018 g KOH+1.1042 g LiOH•H_2O	0.1655 g $K_3[Fe(CN)_6]$+0.3058 g Na_2MoO_4•$2H_2O$
A+10 mM $[Fe(CN)_6]^{3-}$+1.0 wt% Na_2MoO_4	9.9018 g KOH+1.1042 g LiOH•H_2O	0.1655 g $K_3[Fe(CN)_6]$+ 0.6116 g Na_2MoO_4•$2H_2O$
A+10 mM $[Fe(CN)_6]^{3-}$+1.5 wt% Na_2MoO_4	9.9018 g KOH+1.1042 g LiOH•H_2O	0.1655 g $K_3[Fe(CN)_6]$+ 0.9175 g Na_2MoO_4•$2H_2O$
A′+10 mM $[Fe(CN)_6]^{3-}$+1.0 wt% Na_2MoO_4	6.6012 g KOH+1.1042 g LiOH•H_2O	0.1655 g $K_3[Fe(CN)_6]$+ 0.5787 g Na_2MoO_4•$2H_2O$
A″+10 mM $[Fe(CN)_6]^{3-}$+1.0 wt% Na_2MoO_4	13.2024 g KOH+1.1042 g LiOH•H_2O	0.1655 g $K_3[Fe(CN)_6]$+ 0.6447 g Na_2MoO_4•$2H_2O$

Note: Volume = 50 mL.

Table S5. Specific capacity (C g^{-1}) and cycling retention (%) of the $8^{\#}$ electrode in A electrolytes with different concentrations of $[Fe(CN)_6]^{3-}$ additives.

Conc.	Current density /（A g^{-1}）							Cycling Retention%/
	1	2	4	8	16	32	64	30 A g^{-1} /10000 cycles
0	501	468	444	411.2	381.8	355.8	256	58
1	572	528	488	440.8	396.6	342.4	222.7	70
5	622	560	512	469.6	423.4	378.9	307.2	61
10	724	618	560	522.4	468.3	422.7	333.4	43
20	1017	760	664	610.4	540.8	479	365.4	37
50	4179	1158	820	638.4	492.6	327.4	94.7	33
100	5097	1254	828	739.2	572.8	448.6	260.5	4.2
200	7926	5130	960	744	1067.2	642.6	299.5	1.6

Table S6 Specific capacity (C g^{-1}) and cycling retention (%) of the AC electrode in A electrolytes with different concentrations of $[Cu(NH_3)_4]^{2+}$ additives.

Conc.	Current density/（A g^{-1}）							Cycling Retention % /
	1	2	4	8	16	32	64	30 A g^{-1} /10000 cycles
0	260	211.6	195.6	183.2	172.8	160	134.5	83
1	265.1	222.6	205.6	189.9	172.6	160.3	140.8	83
5	359	306	280	241.1	225.4	204.2	147.2	81
10	442	338	308	283	256	235.6	197.1	100
20	564	320	268	210.5	194.1	167.4	133.8	72

Table S7 The active mass ratios of AC anode/811-8# cathode for SCs

SCs	Q_m (C g^{-1})/ (1 A g^{-1})							***m*-/*m*+**	***T*** / ℃
	AC			811-8#					
	A	A+10mM $[Cu(NH_3)_4]^{2+}$	B+10 mM $[Cu(NH_3)_4]^{2+}$	A	A+10 mM $[Fe(CN)_6]^{3-}$(+Na_2MoO_4)	A+20 mM $[Fe(CN)_6]^{3-}$	C+10 mM $[Fe(CN)_6]^{3-}$		
Ⅰ		442			724			**1.6/1**	25
Ⅱ		442				1017		**2.3/1**	25
Ⅲ			434		724			**1.7/1**	25
Ⅳ		442					168	**1/2.6**	25
Ⅴ			434				168	**1/2.6**	25
Ⅵ	260			501				**1.9/1**	25
Ⅰ		442			724			**1.6/1**	-20
Ⅰ		442			724			**1.6/1**	50
Ⅶ		442			724			**1.6/1**	50
Ⅷ		442			724			**1.6/1**	50
Ⅸ		442			724			**1.6/1**	50
Ⅹ		442			724			**1.6/1**	50
Ⅺ		442			724			**1.6/1**	50

Table S8 The specific electrolytes of AC anode and 811-8# cathode for SCs

SCs	AC	811-8#
Ⅰ	A+10 mM $[Cu(NH_3)_4]^{2+}$	A+10 mM $[Fe(CN)_6]^{3-}$
Ⅱ	A+10 mM $[Cu(NH_3)_4]^{2+}$	A+20 mM $[Fe(CN)_6]^{3-}$
Ⅲ	B+10 mM $[Cu(NH_3)_4]^{2+}$	A+10 mM $[Fe(CN)_6]^{3-}$
Ⅳ	A+10 mM $[Cu(NH_3)_4]^{2+}$	C+10 mM $[Fe(CN)_6]^{3-}$
Ⅴ	B+10 mM $[Cu(NH_3)_4]^{2+}$	C+10 mM $[Fe(CN)_6]^{3-}$
Ⅵ	A	A
Ⅶ	A+10 mM $[Cu(NH_3)_4]^{2+}$	A+10 mM $[Fe(CN)_6]^{3-}$+0.5 wt% Na_2MoO_4
Ⅷ	A+10 mM $[Cu(NH_3)_4]^{2+}$	A+10 mM $[Fe(CN)_6]^{3-}$+1.0 wt% Na_2MoO_4
Ⅸ	A+10 mM $[Cu(NH_3)_4]^{2+}$	A+10 mM $[Fe(CN)_6]^{3-}$+1.5 wt% Na_2MoO_4
Ⅹ	A+10 mM $[Cu(NH_3)_4]^{2+}$	A′+10 mM $[Fe(CN)_6]^{3-}$+1.0 wt% Na_2MoO_4
Ⅺ	A+10 mM $[Cu(NH_3)_4]^{2+}$	A″+10 mM $[Fe(CN)_6]^{3-}$+1.0 wt% Na_2MoO_4

Table S9 Ragone and cycling behavior of SCs at room temperature.

SCs	Energy density/ Wh kg^{-1}	Power density/ kW kg^{-1}	Cycling Retention%
Ⅰ	62.95-15.64	0.28-9.07	79%/10000/20 A g^{-1} 88%/10000/20 A g^{-1*}
Ⅱ	54.3-6.86	0.24-7.53	100%/10000/20 A g^{-1}
Ⅲ	54.14-1.42	0.27-8.53	100%/10000/20 A g^{-1}
Ⅳ	22.20-5.31	0.71-11.37	75%/10000/5 A g^{-1}
Ⅴ	11.62-3.54	0.73-11.64	142%/10000/4 A g^{-1}
Ⅵ	20.55-9.23	0.26-8.31	14%/10000/20 A g^{-1}

Note: * the value is based on the 30^{th} cycle.

Table S10. A comparison for the performance of the SCs in the study with some reported SCs.

SCs	Electrolytes	Working voltage / V	Energy density / Wh kg^{-1}	Power density / kW kg^{-1}	Cycling behavior / retention%, cycles, current density	Refs.
			SCs without redox electrolytes			
K-Ni-Co-F//AC	3 M KOH+0.5 M LiOH	1.5	42.7	0.242	98%/10000/4 A g^{-1}	1
K-Co-Mn-F//AC	3 M KOH+0.5 M LiOH	1.5	8	0.14	90%/10000/5A g^{-1}	2
$Co(OH)_2$//GO	1 M KOH	1.2	11.94	2.54	/	3
MnO_2//AC	0.5 M K_2SO_4	1.8	28.4	0.15	94%/23000/10 C	4
$Ni(OH)_2$//AC	1 M KOH	1.3	35.7	0.49	81%/10000/50 mV s^{-1}	5
Co_3O_4//NPC	6 M KOH	1.6	36	1.6	89%/2000/5 A g^{-1}	6
Ni–Zn–Co oxide/hydroxide//AC	6 M KOH	1.5	16.62	2.9	84%/1000/2A g^{-1}	7
$NiCo_2O_4$//RGO	6 M KOH	1.3	23.9	0.65	93.5%/10000/5 A g^{-1}	8
$NiCo_2O_4$@MnO_2//AC	1 M NaOH	1.5	35	0.163	71%/5000/18 mA cm^{-2}	9
CQDs/$NiCo_2O_4$//AC	2 M KOH	1.5	27.8	0.128	101.9%/5000/3 A g^{-1}	10
rGO/$NiCo_2O_4$//AC	2 M KOH	1.3	23.32	0.325	83%/2500/2A g^{-1}	11
			SCs with redox electrolytes			
AC//AC	2 M KOH+0.050 g PPD	1	19.86	17	94.5%/4000/1 A g^{-1}	12
AC//AC	1 M Na_2SO_4+0.1 M $Fe(CN_6)^{3+}$/ $Fe(CN_6)^{4+}$	2	19.8	11.5	80%/7000/30 mA cm^{-2}	13
AC//AC	1 M KBr+0.1 M $MVCl_2$	1.4	51	0.52	30%/300/0.5 A g^{-1}	14
rGO//rGO	1 M KOH+0.05 M KI	0.8	44	/	81%/5000/0.83 A g^{-1}	15

AC//AC	1.2 M $K_3Fe(CN)_6$	0.8	28.3	<0.1	80%/9000/1 A g^{-1}	16
PANI//PANI	1 M H_2SO_4+0.8 M Fe^{3+}/Fe^{2+}	0.8	22.1	0.774	93%/10000/5 A g^{-1}	17
AC//AC	1.2 M $EVBr_2$+0.12 M TBABr+2.88 M NaBr	1.35	64	>3	90%/5000/2 A g^{-1}	18
AC//AC	1 M H_2SO_4+0.03 M viologen	0.9	23		130%/1000/2.5 A g^{-1}	19
AC//AC	1 M H_2SO_4+0.08 M KBr	0.8	11.6		100%/4000/5 mA cm^{-2}	20
AC//AC	1 M H_2SO_4+0.3 g $VOSO_4$	0.8	13.7	0.325	97.6%/4000/5 mA cm^{-2}	21
FAC//FAC	2 M KOH+0.04 M $K_3Fe(CN)_6$	0.6	23.9	1	90%/2000/1 A g^{-1}	22
AC//KNCMF-811(8#)	**3 M KOH + 0.5 M LiOH+10 mM $[Cu(NH_3)_4]^{2+}$//3 M KOH + 0.5 M LiOH+10 mM $[Fe(CN)_6]^{3-}$**	**1.5**	**62.95 54.94 45.94 33.04 26.36 15.64**	**0.28 0.57 1.13 2.22 4.49 9.07**	**79%/10000/20 A g^{-1} (based on the 1st cycle) 88%/10000/20 A g^{-1} (based on the 30th cycle)**	**This work**

Table S11 Ragone and cycling behavior of SCs at low and high temperatures.

Temperature	SCs	Energy density/ Wh kg^{-1}	Power density/ kW kg^{-1}	Cycling Retention%/ 20 A g^{-1} /5000 cycles
-20 ℃	I	36.81-3.18	0.14-1.73	72*
50 ℃	I	70.08-17.38	0.29-9.37	29
	Ⅶ	52.17-11.35	0.28-9.12	58
	Ⅷ	67.19-15.8	0.3-9.48	61
	Ⅸ	44.12-19.15	0.27-8.61	31
	Ⅹ	38.75-12.21	0.26-8.45	28
	Ⅺ	53.94-17.04	0.27-8.65	41

Note: * 10000 cycles

Table S12 Chemicals, reagents and materials used in the study.

Chemials, Reagents and Materials	Type	Company	Characteristics
$NiCl_2•6H_2O$	AR	SinoPharm	purity≥98.0%
$CoCl_2•6H_2O$	AR	SinoPharm	purity≥99.0%
$MnCl_2•4H_2O$	AR	SinoPharm	purity≥99.0%
$KF•2H_2O$	AR	SinoPharm	purity≥99.0%
PVP-K30	GR	SinoPharm	/
$CuSO_4•5H_2O$	AR	Tianjin Fengchuan Chemical Reagent	purity≥99.0%
$K_3[Fe(CN)_6]$	AR	Changsha Fenlukou Reagent	purity≥99.5%
$NH_3•H_2O$	AR	Xilong Scientific	*w*: 25%-28%
KOH	AR	SinoPharm	purity≥85.0%
$LiOH•H_2O$	AR	SinoPharm	purity≥95.0%
KCl	AR	SinoPharm	purity≥99.5%
KNO_3	AR	Xilong Scientific	purity≥99.0%
EG	AR	SinoPharm	purity≥99.0%
NBA	AR	SinoPharm	purity≥99.5%
NPA	AR	SinoPharm	purity≥99.0%
AC	YEC 8a	FuZhou YiHuan	D50: ~10 μm; Density: >0.4 g cm^{-3}; SSA:2000~2500 $m^2 g^{-1}$
AB	Battery grade	/	/
NMP	AR	Kermel	purity≥99.0%
PVDF	Battery grade	/	/
Nickel foam	Battery grade	Tianjin Aiweixin Chemical Technology	Thickness: 1.5 mm
Proton exchange membrane	N115	Dupont	Thickness: 127 μm

References

[1] R. Ding, X. D. Li, W. Shi, Q. L. Xu, X. L. Han, Y. Zhou, W. F. Hong and E. H. Liu, Perovskite $KNi_{0.8}Co_{0.2}F_3$ nanocrystals for supercapacitors, *J. Mater. Chem. A*, 2017, **5**, 17822-17827.

[2] W. Shi, R. Ding, X. D. Li, Q. L. Xu, D. F. Ying, Y. F. Huang and E. H. Liu, Bimetallic Co-Mn Perovskite Fluorides as Highly-Stable Electrode Materials for Supercapacitors, *Chem. Eur. J.*, 2017, **23**, 15305-15311.

[3] R. R. Salunkhe, B. P. Bastakoti, C.-T. Hsu, N. Suzuki, J. H. Kim, S. X. Dou, C.-C. Hu and Y. Yamauchi, Direct growth of cobalt hydroxide rods on nickel foam and its application for energy storage, *Chem. Eur. J.*, 2014, **20**, 3084-3088.

[4] Q. T. Qu, P. Zhang, B. Wang, Y. H. Chen, S. Tian, Y. P. Wu and R. Holze, Electrochemical performance of MnO_2 nanorods in neutral aqueous electrolytes as a cathode for asymmetric supercapacitors, *J. Phys. Chem. C*, 2009, **113**, 14020-14027.

[5] H. B. Li, M. H. Yu, F. X. Wang, P. Liu, Y. Liang, J. Xiao, C. X. Wang, Y. X. Tong and G. W. Yang, Amorphous nickel hydroxide nanospheres with ultrahigh capacitance and energy density as electrochemical pseudocapacitor materials, *Nat. Commun.*, 2013, **4**, 1894.

[6] R. R. Salunkhe, J. Tang, Y. Kamachi, T. Nakato, J. H. Kim and Y. Yamauchi, Asymmetric supercapacitors using 3D nanoporous carbon and cobalt oxide electrodes synthesized from a single metal–organic framework, *ACS nano*, 2015, **9**, 6288-6296.

[7] H. L. Wang, Q. M. Gao and J. Hu. Asymmetric capacitor based on superior porous Ni–Zn–Co oxide/hydroxide and carbon electrodes, *J. Power Sources*, 2010, **195**, 3017-3024.

[8] H. C. Chen, J. J. Jiang, L. Zhang, T. Qi, D. D. Xia and H. Z. Wan, Facilely synthesized porous $NiCo_2O_4$ flowerlike nanostructure for high-rate supercapacitors, *J. Power Sources*, 2014, **248**, 28-36.

[9] K. B. Xu, W. Y. Li, Q. Liu, B. Li, X. J. Liu, L. An, Z. G. Chen, R. J. Zou and J. Q. Hu, Hierarchical mesoporous $NiCo_2O_4$@MnO_2 core–shell nanowire arrays on nickel foam for aqueous asymmetric supercapacitors, *J. Mater. Chem. A*, 2014, **2**, 4795-4802.

[10] Y. R. Zhu, Z. B. Wu, M. J. Jing, H. S. Hou, Y. C. Yang, Y. Zhang, X. M. Yang, W. X. Song, X. N. Jia and X. B. Ji, Porous $NiCo_2O_4$ spheres tuned through carbon quantum dots utilised as advanced materials for an asymmetric supercapacitor, *J. Mater. Chem. A*, 2015, **3**, 866-877.

[11] X. Wang, W. S. Liu, X. H. Lu and P. S. Lee, Dodecyl sulfate-induced fast faradic process in nickel cobalt oxide–reduced graphite oxide composite material and its application for asymmetric supercapacitor device, *J. Mater. Chem.*, 2012, **22**, 23114-23119.

[12] J. H. Wu, H. J. Yu, L. Q. Fan, G. G. Luo, J. M. Lin and M. L. Huang, A simple and high-effective electrolyte mediated with *p*-phenylenediamine for supercapacitor, *J. Mater. Chem.*, 2012, **22**, 19025-19030.

[13] J. Y. Hwang, M. P. Li, M. F. El-Kady and R. B. Kaner, Next-Generation Activated Carbon Supercapacitors: A Simple Step in Electrode Processing Leads to Remarkable Gains in Energy Density, *Adv. Funct. Mater.*, 2017, **27**, 1605745.

[14] S.-E. Chun, B. Evanko, X. F. Wang, D. Vonlanthen, X. L. Ji, G. D. Stucky and S. W. Boettcher, Design of aqueous redox-enhanced electrochemical capacitors with high specific energies and slow self-discharge, *Nat. Commun.*, 2015, **6**, 7818.

[15] K. V. Sankar, R. K. Selvan. Improved electrochemical performances of reduced graphene oxide based supercapacitor using redox additive electrolyte, *Carbon*, 2015, **90**, 260-273.

[16] J. Lee, S. Choudhury, D. Weingarth, D. Kim and V. Presser, High performance hybrid energy storage with potassium ferricyanide redox electrolyte, *ACS Appl. Mater. Interfaces*, 2016, **8**, 23676-23687.

[17] L. J. Ren, G. N. Zhang, Z. Yan, L. P. Kang, H. Xu, F. Shi, Z. B. Lei and Z. H. Liu, High capacitive property for supercapacitor using Fe^{3+}/Fe^{2+} redox couple additive electrolyte, *Electrochim. Acta*, 2017, **231**, 705-712.

[18] S. J. Yoo, B. Evanko, X. F. Wang, M. Romelczyk, A. Taylor, X. L. Ji, S. W. Boettcher and G. D. Stucky, Fundamentally addressing bromine storage through reversible solid-state confinement in porous carbon electrodes: design of a high-performance dual-redox electrochemical capacitor, *J. Am. Chem. Soc.*, 2017, **139**, 9985-9993.

[19] S. Sathyamoorthi, M. Kanagaraj, M. Kathiresan, V. Suryanarayanan and D. Velayutham, Ethyl viologen dibromide as a novel dual redox shuttle for supercapacitors, *J. Mater. Chem. A*, 2016, **4(12)**, 4562-4569.

[20] S. T. Senthilkumar, R. K. Selvan, Y. S. Lee and J. S. Melo, Electric double layer capacitor and its improved specific capacitance using redox additive electrolyte, *J. Mater. Chem. A*, 2013, **1**, 1086-1095.

[21] S. T. Senthilkumar, R. K. Selvan, N. Ponpandian, J. S. Melo and Y. S. Lee, Improved performance of electric double layer capacitor using redox additive (VO^{2+}/VO_2+) aqueous electrolyte, *J. Mater. Chem. A*, 2013, **1**, 7913-7919.

[22] G. X. Wang, M. Y. Zhang, H. F. Xu, L. Lu, Z. Y. Xiao and S. Liu, Synergistic interaction between redox-active electrolytes and functionalized carbon in increasing the performance of electric double-layer capacitors, *J. Energy Chem.*, 2018, **27**, 1219-1224.